A FFM analysis on mode III static and fatigue crack initiation from sharp V-notches

A FFM analysis on mode III static and fatigue crack initiation from sharp V-notches

Alberto Campagnolo[a], Alberto Sapora[b,*]

[a]*Department of Industrial Engineering, University of Padova, Via Venezia, 1, 35131 Padova, Italy*

[b] *Department of Structural, Geotechnical and Building Engineering, Politecnico di Torino, Corso Duca degli Abruzzi 24, 10129 Torino, Italy*

[*]Corresponding author. E-mail address: alberto.sapora@polito.it (A. Sapora).

Abstract

The brittle or quasi-brittle failure initiation at sharp V-notches under mode III loading conditions is investigated by means of the coupled Finite Fracture Mechanics (FFM) approach. The model is developed by assuming that failure is shear stress governed, and by imposing a condition of consistency of both energy and stress requirements. The expression for the notch fracture toughness, which results a function of the material torsional strength, mode III fracture toughness and notch opening angle, is firstly derived. This allows to achieve the dimensionless failure stress through the analytical shape functions presented in the literature. By considering, as a general rule, the transition of fracture mechanism from tensile to shear in terms of the material strength ratio, experimental data referring to cylindrical V-notched samples are then discussed in the static regime. Although FFM predictions on the failure stress are fairly accurate, thus revealing simple tools for engineering purposes, a linear elastic analysis results simplistic since it disregards non linear effects (friction/ductility) observed during tests. Finally, the approach is extended to the fatigue framework, where the basic assumptions are proved to be more reliable. The analysis includes a discussion on the material properties to be implemented, and a satisfactory comparison with a large variety of experimental data.

Keywords: V-notches; mode III; Finite Fracture Mechanics; shearing stresses; fatigue limit.

Nomenclature

a	notch depth
$\bar{a}$	dimensionless notch depth
c	crack length at the notch root

E Young's modulus

G energy release rate

G_c fracture energy

K_I mode I stress intensity factor

K_{III} mode III stress intensity factor

K_{Ic} mode I fracture toughness

K_{IIIc} mode III fracture toughness

K^V_{III} notch stress intensity factor

$\Delta K_{I,th}$ threshold value of the mode I SIF range

$\Delta K_{III,th}$ threshold value of the mode III SIF range

k_3 dimensionless shape function for sharp V-notches under mode III

l_c crack advance

$l_{ch,III}$ mode III characteristic crack length (static fracture)

$l_{th,III}$ mode III threshold crack length (fatigue failure)

R net-section radius of a sharp V-notched bar

R_L nominal load ratio

α proportionality coefficient between K_{IIIc} and K_{Ic} (or between $\Delta K_{III,th}$ and $\Delta K_{I,th}$)

λ_{III} mode III linear elastic eigenvalue

ν Poisson's coefficient

ρ notch root radius

σ_c tensile strength

τ nominal shearing stress

τ_c torsional strength

τ_f critical value of the nominal shearing stress at fracture initiation at the tip of a sharp V-notch under mode III loading

$\Delta\tau_0$ fatigue limit for plain specimens under torsion in terms of stress range

ω notch angle

1. Introduction

The coupled criterion of Finite Fracture Mechanics (FFM) was introduced a couple of decades ago [1,2] to assess the brittle or quasi-brittle failure behaviour of notched elements, thus overcoming the drawbacks rising from Linear Elastic Fracture Mechanics (LEFM). The approach requires for crack onset the simultaneous fulfilment of two conditions: a stress requirement and the energy balance. Accordingly, the critical distance l_c results a structural parameter, depending both on the material properties and the geometry under investigation.

Indeed, criteria involving an internal length and based on either stress or energy requirements had been proposed even before [3–6], falling in the field of Theory of Critical Distances (TCD). If, on one hand, these criteria allow to overcome the limits of LEFM, on the other hand they fail in predicting the failure stress of a notched or cracked structure with size comparable to the critical distance l_c. This is due to the assumption that TCD critical distance l_c is a material constant. With respect to TCD context, FFM can be seen as a step forward to the investigation of brittle fracture in notched elements.

FFM had been originally introduced and applied to defects subjected to mode I loading conditions [1,7,8], then extended to mode II [9,10] and mixed mode I+II [11–14]. Recently, the criterion was assessed under mixed I+II+III loading conditions [15,16]: in a former work [15], it was found that the maximum value of the energy release rate (ERR) is always obtained along the V-notch bisector, contrary to some experimental observations. The authors concluded that ERR cannot determine failure initiation direction for dominant mode III loading. In a subsequent work [16], the failure initiation orientation was determined solely by stress considerations, and the load at fracture was evaluated by both ERR and stress requirements. The analysis was validated by an experimental campaign on three different materials: Macor, PMMA and graphene. Based on these results, the coupled stress-energy criterion was later applied to assess the crack front segmentation under mode I+III loading [17]. Through a numerical study, the authors were able to predict the crack initiation shape, orientation and spacing of the facets ahead of a parent crack.

The goals of this paper are substantially two: to extend the FFM criteria under pure mode III loading conditions through a semi-analytical approach involving shearing stresses; to understand under which circumstances the model can be applied to real practical situations, verifying its validity through a comparison with the experimental data available in the literature. The analysis covers both the static and fatigue regimes, the latter being of one of latest FFM applications [18,19].

Let us introduce the problem under investigation by referring to a sharp V-notched plate under torsional loading, Fig. 1. The FFM approach proposed by Leguillon [1] can be generalized as follows:

$$\begin{cases} \tau_{yz}\left(x = l_c\right) = \tau_c \\ \dfrac{1}{l_c}\displaystyle\int_0^{l_c} K_{III}^2(c)dc = K_{IIIc}^2 \end{cases} \tag{1a}$$

where τ_{yz} is the shear stress field, τ_c is the torsional strength, K_{III} is the mode III stress intensity factor (SIF) related to a small crack of length c at the notch root, and K_{IIIc} is its critical value i.e., the mode III fracture toughness. The first equation in system (1a) represents a stress requirement, whereas the second one describes the energy balance, linking, through Irwin's relationships, the average energy release rate $G=K_{III}^2 / [(1-\nu)E']^2$ to the fracture energy $G_c= K_{IIIc}^2 / [(1-\nu)E']^2$, where $E'=E / (1-\nu^2)$, E being the Young's modulus and ν the Poisson's ratio of the material.

On the other hand, the FFM approach presented by Carpinteri et al. [7] can be rewritten as:

$$\begin{cases} \dfrac{1}{l_c}\displaystyle\int_0^{l_c} \tau_{yz}\left(x\right) dx = \tau_c \\ \dfrac{1}{l_c}\displaystyle\int_0^{l_c} K_{III}^2(c)dc = K_{IIIc}^2 \end{cases} \tag{1b}$$

Both FFM approaches (1a) and (1b) are hence described by a system of two equations in two unknowns: the critical crack advance l_c, and the failure stress τ_f (i.e. the critical value of the nominal stress τ at fracture initiation) entering the expressions for the stress field τ_{yz} and the SIF K_{III}.

According to Eqs. (1a) and (1b) it is assumed that:

1. the material behaviour is assumed as linear-elastic at failure conditions, $\tau = \tau_f$;
2. crack initiation is driven by shear stresses;
3. crack initiates along the bisector line;
4. the crack length l_c is small if compared to the notch depth a.

These simplified assumptions will be discussed more in details in Sections 3 and 4, when referred to a notched cylindrical geometry. Please, note that hypothesis 4 allows to justify the asymptotic approach presented in Section 2.

It is important to underline that the two FFM criteria (1a) and (1b) differ only for what concerns the stress requirement, since the same energetic condition is implemented. Particularly, the criterion (1a) involves a point stress (PS) value, whereas the approach (1b) involves the average stress (AS) value: the criteria will be henceforth named as FFM-PS and FFM-AS, for the sake of brevity. FFM has been recently proved to furnish close predictions to the well-consolidated Cohesive Zone Model (CZM), once the constitutive law is properly defined [20–22]. Indeed, FFM-PS provides close predictions to the CZM once a Dugdale (cohesive) law is assumed, whereas FFM-AS achieves similar results to the CZM implemented through a linear softening cohesive law.

Fig. 1. V-notched plate under mode III loading conditions.

2. Shallow sharp V-notched structures

The notch stress intensity factor (NSIF) K_{III}^{V} represents the coefficient of the dominant term of the stress field at the notch tip and it is defined by the relationship:

$$K_{III}^{V} = \lim_{x \to 0} \left[\tau_{yz}(x) \cdot (2\pi x)^{1-\lambda_{III}} \right] \tag{2}$$

where λ_{III} represents the eigenvalue provided by Qjan and Hasebe [23]:

$$\lambda_{III} = \frac{\pi}{2\pi - \omega} \tag{3}$$

Within brittle structural behaviour, K_{III}^{V} can be reasonably assumed as the governing failure parameter and the failure condition under mode III loading conditions can be thus expressed as:

$$K_{III}^{V} = K_{IIIc}^{V} \tag{4}$$

K_{IIIc}^{V} being the critical NSIF (or notch fracture toughness).

In case of a semi-infinite V-notched slab (a being the notch depth) under out-of-plane shearing loading conditions, once the nominal stress τ has been defined (Fig. 1), we have that

$$K_{III}^{V}(a) = k_3(\omega) a^{1-\lambda_{III}} \tau \tag{5}$$

The shape function k_3 related to the geometry under investigation was evaluated by Zappalorto et al. [24]: in case of shallow notches, as the present one (a being the only relevant geometrical parameter), k_3 results a function only of the notch angle ω. More in details, according to definition (2) for the NSIF, k_3 varies from $\sqrt{\pi}$ for the crack case (ω = 0°, $K_{III}^{V} = K_{III} = \tau\sqrt{\pi a}$), to 1 for the unnotched geometry (ω = 180°, $K_{III}^{V} = \tau$).

On the other hand, in order to implement the FFM criteria by Eqs. (1a,b), the stress field and the SIF functions for the present geometry have to be known. According to hypothesis 4 of Section 1, they can be approximated, respectively, by the following asymptotic relationships

$$\tau_{yz}(x) = \frac{K_{III}^{V}}{(2\pi x)^{1-\lambda_{III}}} \tag{6}$$

and

$$K_{III}(c) = \Lambda(\omega) K_{III}^{V} c^{\lambda_{III}-0.5} \tag{7}$$

An analytical expression was proposed for Λ in Eq. (7) by Duan et al. [25]. According to notation (2), it can be expressed as

$$\Lambda(\omega) = \sqrt{\frac{\pi}{\lambda_{III}(2\pi)^{2(1-\lambda_{III})}}} \tag{8}$$

The functions k_3, λ_{III} and Λ are plotted in Fig. 2 as a function of the notch angle ω, together with their corresponding counterparts for mode I loading conditions (β, λ_I and μ if referred to the nomenclature adopted in Sapora et al. [19], respectively).

It is worth noting that the mode III stress fields of cracks initiated either at the tip of sharp or blunt notches have been derived analytically by Salviato et al. [26], and by Zappalorto et al. [27], respectively.

Fig. 2. Notch angle dependent functions implemented in the present study: λ_{III}, k_3 and Λ. The dotted lines refer to the corresponding functions for mode I loading conditions [19].

Substituting Eqs. (6) and (7) into the systems described by Eqs. (1a, b), yields:

$$K_{IIIc}^{V} = \varsigma(\omega) l_{ch,III}^{1-\lambda_{III}} \tau_c \tag{9}$$

where

$$l_{ch,III} = \left(\frac{K_{IIIc}}{\tau_c} \right)^2 \tag{10}$$

and where the function ς takes on a different form depending on the FFM criterion adopted. If the philosophy proposed by Leguillon [1] is implemented through Eq. (1a), we have that:

$$\varsigma(\omega) = \left(2\lambda_{III}\right)^{2(1-\lambda_{III})} \tag{11a}$$

On the other hand, the approach by Carpinteri et al. [7] via Eq. (1b) yields:

$$\varsigma(\omega) = 2^{2(1-\lambda_{III})}\lambda_{III} \tag{11b}$$

The two functions ς according to Eqs. (11a,b) are plotted in Fig. 3: again it is shown the comparison with the case of mode I loading conditions, where the function was termed ξ [19].

Fig. 3. Function ς according to different FFM criteria, see Eq. (11a) and (11b), respectively. The dotted lines refer to the case of mode I loading conditions [19].

The second unknown of FFM systems (1a) and (1b) is represented by the critical crack advance l_c. It takes the following form according to Eq. (1a):

$$l_c = \frac{2}{\pi}\lambda_{III}^2 l_{ch,III} \tag{12a}$$

varying between $1/(2\pi)\ l_{ch,III}$ for the cracked case ($\omega = 0°$) to $2/\pi\ l_{ch,III}$ for the un-notched geometry ($\omega = 180°$), whereas it results surprisingly constant according to Eq. (1b):

$$l_c = \frac{2}{\pi} l_{ch,III} \tag{12b}$$

Thus, the present geometry is similar to the Griffith crack case analysed by Cornetti et al. [2] (see also Sapora et al. [18]): FFM-AS reverts to the average stress criterion proposed by Taylor [4], and also the two critical distances coincide.

At incipient failure ($\tau = \tau_f$), upon substitution of Eqs. (5) and (9) into condition (4), one gets:

$$\frac{\tau_f}{\tau_c} = \frac{\varsigma}{k_3 \bar{a}^{1-\lambda_{III}}} \tag{13}$$

where $\bar{a} = a / l_{ch,III}$ is the dimensionless notch depth.

Equation (13) can be modified to take short notches into account by inserting a parameter $\bar{a}_0^V$ in order to recover $\tau_f \to \tau_c$ as $a \to 0$, similarly to what proposed by Atzori et al. [28] for mode I loadings. In formulae:

$$\frac{\tau_f}{\tau_c} = \frac{\varsigma}{\left(k_3^{\frac{1}{1-\lambda_{III}}} \bar{a} + \bar{a}_{0,III}^V \right)^{1-\lambda_{III}}} \tag{14}$$

where $\bar{a}_{0,III}^V = \varsigma^{\frac{1}{1-\lambda_{III}}}$. Predictions according to Eqs. (13) and (14) are reported in Fig. 4 for different notch angles ω by means of Eq. (11b).

Once the angle has been set at 90°, Fig. 5 shows the comparison between the two different FFM criteria: as it is well-consolidated [7], the average criterion (1b) provides the most conservative predictions. The same figure also shows the FFM-AS results related to mode I loading conditions [18]. For very brittle materials, the following simplifying hypothesis can be assumed $\sigma_c \approx \tau_c$ [10]. Furthermore, since $K_{Ic} = \sqrt{(G_c E')}$, whereas $K_{IIIc} = \sqrt{[(1-\nu) G_c E']}$, it can be argued that:

$$K_{IIIc} = \alpha K_{Ic} \tag{15}$$

with $\alpha = \sqrt{1-\nu}$. In Figure 5 mode I results are normalized through Eq. (15) by setting $\nu = 0.3$, and thus $\alpha \approx 0.84$. It is important to mention that Eq. (15) holds from a theoretical point of view. From a realistic point of view, frictional effects and crack face asperities generally lead to higher α values [29]. This aspect will be investigated more in details in Section 4, when dealing with torsional fatigue.

Fig. 4. V-notches under torsion: FFM-AS predictions for different notch angles according to Eqs. (13) (continuous line) and (14) (dotted line) coupled with Eq. (11b).

Fig. 5. V-notches under torsion, ω = 90°: predictions according to FFM-PS (thin line) and FFM-AS (thick line). The dotted line refers to mode I predictions via FFM-AS, provided that $\sigma_c = \tau_c$ and $K_{Ic} = 1.2\, K_{IIIc}$.

2.1 Finite sharp V-notched structures

For finite geometries, the analysis presented above still holds true, but for the shape function k_3 in Eq. (5). Indeed, it refers to the particular structure under investigation (depending, besides on the notch angle, on the geometry and the size of the notched component too) and must be generally evaluated through a Finite Element Analysis (FEA). In Zappalorto et al. [24] the following relationship was proposed instead of (5):

$$K_{III}^{V}(a) = k_3(\omega, a/R) R^{1-\lambda_{III}} \tau \tag{16}$$

R being the ligament depth and τ the nominal shearing stress on the net sectional area. The shape functions k_3 were evaluated every 30° over the range $1/20 \leq a/R \leq 1$, and they are reported in Appendix A, for the sake of completeness. Note that: i) for lower a/R ratios the notch can be considered shallow, and Eq. (5) can be applied without loss of accuracy; ii) for intermediate notch amplitudes, a linear interpolation can be exploited as suggested by Zappalorto et al. [24].

Through Eq. (16), Eq. (13) reduces to:

$$\frac{\tau_f}{\tau_c} = \frac{\varsigma}{k_3 \bar{R}^{1-\lambda_{III}}} \tag{17}$$

where $\bar{R} = R / l_{ch,III}$.

Since the experimental data considered in the next sections all refer to the notched cylindrical geometry (Fig. 6), the FFM energy balance in Eqs. (1a, b) should be generalized as follows (while the stress conditions keep unchanged):

$$\int_0^{l_c} K_{III}^2(c)\, 2\pi(R-c)\, dc = K_{IIIc}^2 \left(\pi R^2 - \pi (R - l_c)^2 \right) \tag{18}$$

where R is the radius of the net section for the solid round bar. However, in case that the crack advance l_c is sufficiently small with respect to the radius R, Eq. (18) reduces to the second condition in Eqs. (1a, b), and the analysis presented above still holds true without loss of accuracy.

Before proceeding, let us remind that the present FFM analysis refers to sharp V-notches, i.e. $\rho = 0$ in Fig. 6. This assumption can be extended also to real notches (as it will be done in the following Sections), provided that the notch radius ρ is small compared to the critical distance l_c. Under mode I loading condition, it was proved that, as long as $\rho/l_{ch,I} < 0.1$, with $l_{ch,I} = (K_{Ic}/\sigma_c)^2$, the deviations keep below 2% even for the crack case [30]. Note that the influence of ρ increases as the notch angle decreases. Since $l_{ch,I} < l_{ch,III}$, the radius of curvature under mode III can be supposed to have even less impact: this point has been highlighted in the very recent paper by Santus et al. [31], dealing with mode III critical distance determination to apply TCD approaches. Similar arguments can be assumed in the fatigue framework, provided that $l_{ch,III}$ is replaced by $l_{th,III}$ (Section 4).

Fig. 6 V-notched bar under torsion: 3D view and cross-sectional area.

3. Static fracture

It is well consolidated that, considering a round bar under torsion (Fig. 6), the fracture can be either along a helical path (oriented approximately ±45° to the bar axis) for a brittle material, or in a plane perpendicular to the axis of the bar for a ductile material [32]. The different fracture planes observed for these two materials witness the different fracture mechanism: brittle materials fail due to tensile stresses, whereas ductile materials fail involving shear stresses.

The presence of a crack reasonably affects the structural behaviour. The transition of fracture type in either brittle or ductile cracked solid under mixed-mode I+III loading conditions was investigated by Liu et al. [32]. The authors implemented a simple point stress criterion based on the competition between the maximum normal stress and the maximum shear stress. Particularly, the prediction of the fracture type was determined by comparing τ_{max}/σ_{max} at a critical distance from the crack tip to the material strength ratio τ_c/σ_c. It was proved that the failure mechanism depends both on the mode mixity, and the ratio τ_c/σ_c: the results were corroborated by ad hoc experimental tests carried out on a brittle material (PMMA), and a ductile one (7050 aluminium alloy). On the other hand, restricting the analysis to pure mode III loading conditions, the discriminant is limited to the ratio τ_c/σ_c: as far as $\tau_c \geq \sigma_c$, as it happens for very brittle materials, fracture would undergo a tensile mechanism. On the contrary, the shear mechanism with a flat surface dominates the behaviour for increasingly less brittle materials $\tau_c < \sigma_c$, till the (ductile) limit $\tau_c = 0.5\ \sigma_c$ imposed by Tresca's criterion.

The fracture behaviour and the crack front instability under mixed mode I+III loading has been investigated in detail also in recent works. Lazarus et al. [33-35] attempted to explain the crack front rotation and segmentation by means of 'global type criteria', linked to the disappearance of mode III and consisting in maximizing the mean value of mode I SIF or the mean value of total energy release rate along the front over a critical distance. Despite the good matching with ad-hoc experimental data on PMMA, it was observed that global criteria were difficult to be extended to other geometrical configurations, and local approaches (such as Principle of Local Symmetry or the Maximum Tangential Stress criterion) should be preferred for implementation. Similar arguments hold for fatigue failure. On the basis of both analytical and numerical derivations, subsequent works by Pham and Ravi-Chandar [36,37], Leblond and co-workers [38,39] and Doitrand and Leguillon [17] concluded that cracks subjected to combined modes I+III loading cause fragmentation of the parent crack front without any threshold; mode III perturbations as small as $K_{III}/K_I \sim 0.001$ cause nucleation of fragmented daughter cracks, shaped as flat facets rotated towards the principal stress axis. This result has been corroborated also by experimental data generated by fracture tests on specially designed specimen geometries made of brittle materials, namely glass, Homalite H-100 and gelatin based hydrogel.

Besides the above considerations it should be added that brittleness (ductility) is a structural property and not just a material one. Thus, also the notch or sample sizes play an important role. An interesting contribution in this framework is due to Zehnder and Zella [40], who tested notched circular PMMA rods under torsional loading letting vary the notch depth. As it increases, a transition of the overall fracture surface from spiral to flat was observed.

Furthermore, generalizing the results to sharp V-notches, as the present analysis is focused on, the higher the notch amplitude the higher the related failure loads. Thus, notch angles different from zero lead lo less brittle behaviour than the cracked case. In this sense, the limit $\tau_c/\sigma_c \geq 1$ could reveal less strict. Further investigations are in progress.

3.1 Comparison with experimental data

Looking at the experimental data in the literature, three recent papers investigated sharp V-notched cylindrical specimens under pure torsion. The geometrical dimensions were identical in all tests: a = 2 or 5 mm, once fixed the gross-section radius $a + R$ = 10 mm. Only results related to ρ = 0.1 mm will be analysed in the following, satisfying the requirement of sharp V-notches.

The first study involves polycrystalline graphite [41], V-notches referring to ω = 30° and 120°. Indeed, no comments were provided on the fracture surface and the related crack path. In this work the SED criterion was applied for the first time to mode III loading conditions in order to estimate the fracture load, and theoretical predictions were in good agreement with experimental results.

In the second one, the fracture behaviour of notched round bars made of PMMA at room temperature was investigated by Berto et al. [42]. As regards V-notches, only one angle (ω = 120°) was considered. The experimental campaign presented some drawbacks: notched specimens presented a large plastic behaviour during tests, and the influence of the effective resistant net area was found to be the predominant parameter (instead of the notch shape geometry). Due to the presence of large scale yielding, samples 'exploded' or presented irregular inclined fracture planes with partial detachment of the material: consequently, it was not possible to define the crack path. Note that besides the type of notch and the loading conditions (including the loading control and rate), also the material (molecular weight, additives, etc.) and the manufacturing process of PMMA can play a role on its nonlinear behaviour. The SED criterion was applied for theoretical results by means of a best fit of the experimental data.

In the third work, Berto et al. [43] tested V-notched samples made of PMMA at –60°C with ω =120°. Although the low temperature increased the brittleness structural behaviour, the torque versus angle curves showed a marked non-linear trend. All samples with lower notch depth broke suddenly without evident cracking before the final failure. For reasons similar to the past ones, it was not possible to define precisely the actual crack path at fracture initiation: the topography of the fracture surfaces of the specimens which did not explode at the failure was characterised by irregular inclined fracture planes with partial detachment of the material in the close neighbourhood of the notch tip. With respect to this experimental campaign, SED criterion provides accurate results without the necessity of fitting.

Material	Ref.	σ_c (MPa)	τ_c (MPa)	K_{IIIc} (MPa$\sqrt{m}$)	$l_{ch,III}$ (mm)
Graphite	[41]	27	30	2.42	6.5
	[44]	30	37	1.26	1.2
PMMA	[42]	74	67	3.35	2.5

PMMA –60°C	[43]	128.7	153.1	6.02	1.55

Table 1. Static fracture: mechanical properties of the materials tested in the literature and reported in the related references.

The material properties related to the above materials are reported in Table 1: it is worth noting that the mode III fracture toughness K_{IIIc} was evaluated experimentally for PMMA and PMMA –60°C, whereas it was estimated from the geometry with ω=30° for graphite. For both graphite and PMMA, the resulting value for $l_{ch,III}$ is not small compared to the notch depth, thus undermining the asymptotic approach presented in Section 2. On the contrary, the mechanical properties of graphite were recalculated experimentally in a subsequent work [44], resulting in a higher value of τ_c, a sensibly lower value of K_{IIIc} (estimated from ω = 10°) and, thus, of $l_{ch,III}$ (Table 2).

The presence of non-linearity/plasticity observed during experiments [41–43], as well as the lack of information on the real crack path, make it difficult to state whether or not the present FFM approach leads to reasonable failure predictions.

On one hand, it should be underlined that criteria based on a critical distance could be applied also under moderate and large scale yielding regimes, at least under mode I loading conditions [45–47]. This has already been proved even for the FFM approach [48,49]. A straightforward application of Eq. (17) to experimental data on graphite [41] (by implementing the mechanical properties evaluated in [44]) and PMMA at -60°C [43], for instance, show accurate predictions (see Fig. 7), FFM-AS providing again the most conservative predictions. Results on PMMA are less accurate: the experimental failure stress was higher than the torsional strength, reflecting the drawbacks faced during tests.

Figure 7. Static fracture on V-notched structures: FFM failure stress vs. experimental data.

On the other hand, although the criterion may work, in our opinion the ability of the model to reflect the correct crack path (and thus the correct failure mechanism) is questionable. As can be seen from Table 1, the material strength ratio τ_c/σ_c is always higher than (or very close to) 1. According to our

past comments, this would suggest that the linear elastic fracture should be governed by normal stresses: the lack of evidence in the experimental crack path does not help to corroborate the above conclusion. In any case, for very brittle materials, it should be stressed that plain specimens break under a tensile fracture mechanism. Thus, the value of τ_c recorded experimentally would be affected by a different failure mode than that supposed for notched samples in the present analysis.

Finally, since the observed nonlinearities could be imputable to friction between crack surfaces, this phenomenon should be properly taken into account in the FFM analysis. Further studies are in progress based on the above considerations, which imply to remove the former three hypotheses described in Section 1.

It is important to underline that the Literature presents also many experimental data on V-notched samples subjected to mixed mode I+III loading conditions. Among the others, let us cite the experiments carried out on PMMA by Ayatollahi and Saboori [50] and Torabi et al. [51], and the interesting FFM work by Yosibash and Mittleman [16], involving tests on PMMA, graphite, and macor. In these studies, predominant mode I loading conditions were achieved, and the related modelling analyses were performed coherently through a tensile failure mechanism. Of course, in case of FFM, a semi-analytical investigation cannot be performed due to the difficulties in managing the ERR found by Yosibash and Mittleman [16], previously cited in the Introduction.

4 Fatigue failure

The FFM coupled criterion has been recently applied to predict the fatigue limit of mechanical components subjected to mode I loading conditions and weakened by central sharp cracks and circular holes [18], or by edge sharp V-notches as well as U-notches [19]. In the present section the FFM coupled criterion will be extended to assess the fatigue limit of notched structures subjected to torsional loading. It is worth noting that the crack/notch sensitivity in this framework has been previously investigated by Atzori and Meneghetti [52,53], Susmel and Taylor [54], and by Atzori et al. [55] through other theoretical approaches.

When dealing with torsional fatigue, the extension of the FFM criteria described by Eqs (1a, b) is straightforward:

$$\begin{cases} \Delta\tau_{yz}\left(x=l_c\right)=\Delta\tau_0 \\ \dfrac{1}{l_c}\displaystyle\int_0^{l_c}\Delta K_{III}^2(c)dc=\Delta K_{III,th}^2 \end{cases} \tag{19a}$$

and

$$\begin{cases} \dfrac{1}{l_c}\displaystyle\int_0^{l_c} \Delta\tau_{yz}\left(x\right)dx = \Delta\tau_0 \\ \dfrac{1}{l_c}\displaystyle\int_0^{l_c} \Delta K_{III}^2(c)dc = \Delta K_{III,th}^2 \end{cases} \tag{19b}$$

where $\Delta\tau_0$ represents the fatigue limit or the high-cycle fatigue strength, typically defined at $N_A = 2\ 10^6$ cycles, of the material under torsion loading, and $\Delta K_{III,th}$ is the threshold value of the mode III SIF range, above which propagation of long cracks occurs according to Paris' law.

By considering finite cylindrical notched geometries (Fig. 6), the solution of Eqs. (19a,b) coincides with those related to the static case (Section 2), but extended to the fatigue regime:

$$\frac{\Delta\tau_f}{\Delta\tau_0} = \frac{\varsigma}{k_3\,\bar{R}^{1-\lambda_{III}}} \tag{20}$$

and

$$l_c = \frac{2}{\pi}\lambda_{III}^2 l_{th,III} \tag{21a}$$

according to FFM-PS (where ς is defined by Eq. (11a)) or

$$l_c = \frac{2}{\pi} l_{th,III} \tag{21b}$$

according to FFM-AS (where ς is defined by Eq. (11b)). In the above expressions we have

$$l_{th,III} = \left(\frac{\Delta K_{III,th}}{\Delta\tau_0}\right)^2 \tag{22}$$

and $\bar{R} = R / l_{th,III}$.

It is worth mentioning that the FFM approach under torsion fatigue loading according to Eqs. (19-22) is valid under the following assumptions:

1. the material behaviour is assumed as linear-elastic at the fatigue limit condition;
2. crack initiation is driven by shear stresses both for plain and cracked/notched specimens;
3. crack is assumed to initiate and early propagate by assuming a circumferential shape (Fig. 6);

4. a notch weakening behaviour is assumed, i.e. $\Delta\tau_f < \Delta\tau_0$.

5. l_c is reduced if compared to the net-section radius R.

Dealing with hypothesis 1, it is widely accepted in the literature that linear-elastic approaches can be applied with good approximation to the strength assessment of structural components at the fatigue limit condition, since this typically corresponds to low stress and strain amplitudes. However, the authors are aware of nonlinear phenomena which could affect the torsional fatigue strength of the material, such as plasticity at the crack tip, frictional contact and formation of fretting debris during the tests, also at high-cycle fatigue regime.

Concerning hypothesis 2, crack initiation and early propagation in plain bars made of ductile materials tested under torsion loading near the fatigue limit are mainly mode II dominated at the specimen surface [54,56–58], while propagation into the material is mode III dominated [58–60]. Accordingly, fatigue cracks tend to initiate and propagate on material planes where shear stress is maximum, i.e. along either transverse or longitudinal direction. After the shear crack has reached a critical length, which is a function of the material and of the applied torsion load level [60,61], crack branches and starts to propagate along planes where the range of the normal stress is maximum, i.e. a mode I dominated growth. Even the presence of stress concentrators, such as in the case of cracked or notched bars, crack initiation and propagation are mode II dominated at specimen surface, while it is mode III dominated into the depth of the material. More in detail, many researchers [62–69] have analysed by scanning electron microscopy the fracture surfaces of notched steel bars tested under torsion loading near the fatigue limit and observed a number of small, macroscopically flat regions, i.e. small semi-elliptical cracks initiated by mode III loading ahead of the initial circumferential notch tip. According to Ritchie [63], mode III crack advance can occur through the coalescence, by mode II shear, of cracks initiated at the notch tip. As for plain specimens, after the crack has propagated to certain length, it branches, kinks or twists and the subsequent propagation is mode I dominated, showing a transition to a rough failure mode consisting of peaks and valleys and giving rise to the so-called factory roof type fracture surface [64]. Based on hypothesis 2), the proposed approach does not account for crack propagation phenomena, such as branching and kinking/twisting from a shear crack to a mode I crack, which typically occur when the crack has already reached a macroscopic extension, as documented by many researchers in the literature [62,64,67,69–72]. Tschegg [62,64] tested notched bars made of AISI 4340 and observed that the fatigue crack continued in a macroscopically flat fracture mode up to a crack depth of 0.8 mm. Tanaka [67,69] tested notched bars made of medium carbon steel and stainless steel and observed a flat fracture surface up to a crack depth of 0.030 mm. Also dealing with Ti-6Al-4V notched bars, Meneghetti et al. [70,71] observed a circumferential flat crack having depth

on the order of 0.3-0.4 mm which was located between the notch tip and the factory-roof type fracture surface.

According to hypothesis 3, only mode III radial crack propagation, i.e. towards the centre of the specimen of Fig. 6, is considered; while mode II circumferential crack propagation, i.e. along the surface of the specimen of Fig. 6, is neglected. This is a simplifying hypothesis and it is in agreement with the Finite Fracture Mechanics concept, which assumes the initiation of a finite-size crack neglecting the previous phases, i.e. the initiation of mode III small semi-elliptical cracks and the coalescence under mode II. It is worth mentioning that some researchers, e.g. Pokluda and co-workers [73,74], stated that mode III crack propagation is not possible based on dislocation movements analysis, whereas they believe that only mode I and mode II loadings can generate new crack surfaces, giving rise to crack propagation. However, this is an open point and a shared hypothesis has not yet been reached among the scientific community.

Afterwards, hypothesis 4 states that the fatigue limit of a notched bar is lower than that of a plain specimen. While this is straightforward for notched components under axial loading condition, it could be not always verified under torsion. As a matter of fact, an anomalous notch-strengthening phenomenon has been found by mode III testing cylindrical specimens made of austenitic stainless steel [75], NiCrMo steel [72] and pure titanium [76]: the fatigue strength of notched components reveals higher than that of plain ones. This effect can be explained on the basis of the factory-roof type fracture surfaces found in notched specimens: the sliding contact and the meshing between crack surfaces, that is the interference and interlocking of the opposing fracture surface asperities [64], led to a retarded crack propagation [62–64]. The FFM approach proposed in this paper cannot predict the notch-strengthening phenomenon, being correlated to extrinsic mechanisms acting during crack growth. Therefore, if applied to materials prone to exhibit a notch-strengthening effect, the FFM theoretical predictions will be on the safe side, the estimated torsion fatigue limit being lower than the experimental one.

Finally, it should be noted that the critical distance l_c under torsion is typically larger than that under axial loading up to five times, as observed by several researchers [54,59,71,72,77]. Anyway, the proposed FFM approaches according to Eqs.(19a, b) can be applied provided that l_c is small if compared to the specimen radius R, as stated by hypothesis 5, otherwise torsion stress gradient would be not negligible and should be included in the right-hand side of Eqs. (19a, b). Comparing Eqs. (12a) and (12b) with Eqs. (21a) and (21b), the FFM critical distances in the static and fatigue regimes differ only for the expressions of $l_{ch,III}$ and $l_{th,III}$, defined by Eqs. (10) and (22), respectively. In a future work, it would be interesting to compare these two quantities for the same material. Unfortunately,

the materials considered in the present work have not been tested both under static and loading conditions in the original references to derive (τ_c, K_{IIIc}) and ($\Delta\tau_0$ and $\Delta K_{III,th}$) or the equivalent tensile properties, therefore at the present state-of-the-art $l_{ch,III}$ and $l_{th,III}$ cannot be quantitatively compared for the same material.

The discussion reported above should clarify that the hypotheses behind the proposed FFM approach are just engineering assumptions introduced to simplify the problem, so that it can easily be treated in engineering design practice.

4.1 Estimation of $\Delta K_{III,th}$

In order to validate the present FFM approach against experimental results taken from the literature, two material properties derived under torsion fatigue loading are required to apply Eq. (20): (i) $\Delta\tau_0$, i.e. the fatigue limit or the high-cycle fatigue strength of the plain material, and (ii) $\Delta K_{III,th}$, i.e. the threshold value of the mode III SIF range of the cracked material. Whereas the former can be easily obtained by plain cylindrical specimens under torsional loading and it is usually available in the literature for several materials, it is extremely complex to estimate the latter (please, see also the recent work by Santus et al. [31], who have investigated in detail the procedure to determine the mode III critical distance, providing also numerical procedures to determine the statistical distribution of the material parameters and of the critical distance itself). According to several researchers [60,62,64,67], the practical difficulties in the experimental derivation of $\Delta K_{III,th}$ are mainly related to:

- a threshold for mode III fatigue crack growth can be defined in at least two different ways [65]: (i) the initiation by mode II/III of small elliptical cracks giving rise to macroscopically small flat regions; (ii) the transition from a mode II/III macroscopically flat to a mode I factory roof fracture surface. The last condition occurring long before crack arrest, the corresponding threshold is no longer comparable to that derived under mode I, since crack does not stop, but continues to propagate in a different way;
- an extensive plastic region can be generated at the tip of small cracked bars;
- the frictional contact and interference between the crack surfaces and the load dissipation on crack flanks, which makes the threshold value dependent on the crack length, therefore not an intrinsic material property.
- different results can be obtained as a function of the adopted specimen geometry: slit specimens give lower threshold values as compared to specimens pre-cracked in tension; V-

notched bars even if with the same notch tip radius as the slit specimens, provide higher threshold values than those derived from pre-cracked specimens.

To partially overcome previous difficulties, many researchers have tried to correlate in an engineering manner the mode III threshold value $\Delta K_{III,th}$ to that derived under mode I loading $\Delta K_{I,th}$, which can be measured experimentally following International Standards [78] and it is usually available in the literature for several materials. The resulting expression is reported below, similarly to Eq. (15):

$$\Delta K_{III,th} = \alpha \, \Delta K_{I,th} \tag{23}$$

Concerning the coefficient α, several values based on either analytical or experimental considerations have been proposed in the literature. Starting from analytical investigations, Pook and Sharples [79] suggested α = 1.35 by considering the transition from a macroscopically flat to a factory roof type fracture surface as the mode III threshold condition. On the other hand, dealing with experimental considerations, Pook and Sharples [79] firstly put forward α =1.25 based on experimental threshold values derived from mild steel, while later on he recommended α = 1 as a lower bound for design purposes based on a larger database of experimental results [80]. Susmel and Taylor [54], taking advantage of previous analytical studies performed by Beretta and Murakami [81] proposed α = 0.85, by considering the non-propagation of mode I branched cracks as the mode III threshold condition. Richard et al. [82] suggested α = 1 on the basis of experimental results generated by a ferritic steel, which was prone to mode III crack propagation, while experimental results available on Al 7075-T651 and austenitic steel provided α = 1.60 - 3, since they were more inclined to branch to mode I crack. Finally, on the basis of experimental results from steel bars [67], according to Tanaka et al. [69] it is necessary to distinguish between different thresholds for crack initiation (α = 1) and propagation (α = 2 – 2.40) under torsional fatigue. These different values were correlated to complex phenomena occurring under torsion loading such as extensive plasticity, frictional contact and formation of fretting debris at the crack tip.

Given that there is no agreement in the scientific community, in the present work α = 1 is adopted in agreement with Pook's proposal of a lower bound value useful for an engineering design purpose [80] and with Richard et al. [82]. Moreover, this choice reveals on the safe side in most cases.

Even if the threshold value of the mode I SIF range $\Delta K_{I,th}$ is easier to be measured experimentally as compared to $\Delta K_{III,th}$ and databases are available for several materials [83,84], for some specific materials $\Delta K_{I,th}$ is neither reported in the original papers nor available in databases. To overcome this issue, Atzori et al. [84] proposed some empirical equations to estimate El Haddad's constant a_0 on the basis of a large database of fatigue data found in the literature. Equation (24) reports the definition

of the El Haddad's constant a_0, which depends on $\Delta K_{I,th}$, along with the expression proposed by Atzori et al. [84], which depends on the ultimate tensile stress σ_{UTS} (or equivalently σ_c) and the axial fatigue limit of the plain material $\Delta\sigma_0$. The approximate expression of a_0 provides a correlation factor equal to $R^2 = 0.791$, based on a fitting of steel experimental data:

$$\begin{cases} a_0 = \dfrac{1}{\pi}\left(\dfrac{\Delta K_{I,th}}{\Delta\sigma_0}\right)^2 \\ a_0 \cong \left(\dfrac{99}{\sigma_{UTS}\Delta\sigma_0}\right)^{1.17} \qquad [\text{m}] \end{cases} \tag{24}$$

By coupling previous equations, it is straightforward to derive an equation to approximately estimate the threshold value of the mode I SIF range $\Delta K_{I,th}$, which is valid only for steels [84].

$$\Delta K_{I,th} \cong \sqrt{\pi}\left(\frac{99}{\sigma_{UTS}}\right)^{0.585}\left(\Delta\sigma_0\right)^{0.415} \qquad [\text{MPa}\sqrt{\text{m}}] \tag{25}$$

It is worth noting that the dependency of $\Delta K_{I,th}$ on the load ratio R_L is accounted for by the axial fatigue limit of the plain material, $\Delta\sigma_0$ which must be derived at the required load ratio R_L. The effect of the load ratio R_L on $\Delta K_{I,th}$ can be taken into account also by Eq. (26) proposed by Taylor [83] once $\Delta K_{I,th,RL=0}$ is known:

$$\Delta K_{I,th,R_L} = \begin{cases} \Delta K_{I,th,R_L=0}\cdot\sqrt{\dfrac{1-R_L}{1+R_L}} & if \quad R_L \geq 0 \\ \alpha_R(R_L)\cdot\Delta K_{I,th,R_L=0} & if \quad R_L < 0 \end{cases} \tag{26}$$

In Eq. (26), according to Taylor [83], it is common practice to assume $\alpha_R = 2$ for $R_L = -1$ based on crack closure considerations.

4.2 Comparison with experimental data

After having discussed issues about mode III threshold derivation, the theoretical predictions of the fatigue limit of notched components under torsional loading according to FFM approach (Eqs. (19a,b)) are compared with experimental results taken from the literature. Table 3 summarizes all collected experimental results and details about the considered notch geometries and materials, which include several steel categories (470 MPa $\leq \sigma_{UTS} \leq$ 883 MPa), the austempered ductile iron ADI 900 ($\sigma_{UTS} \approx$ 900 MPa) and the titanium alloy Ti-6Al-4V ($\sigma_{UTS} \approx$ 1000 MPa). Table 3 shows also that all considered experimental results are relevant to less brittle materials, having $\Delta\tau_0/\Delta\sigma_0 < 1$. It is worth

mentioning that, according to the model proposed by Liu et al. [32] to predict the fracture path and modes also in the fatigue regime, a ratio $\Delta\tau_0/\Delta\sigma_0 < 1$ would correspond to a shear fracture mode for a cracked bar under torsion fatigue loading, i.e. the fracture surface should be flat.

The experimental results relevant to V-notched bars having opening angle $\omega = 35°$ were obtained by Quilafku et al. [85] by testing a low carbon steel ($\sigma_{UTS} \approx 500$ MPa). The original work does not include any information or figures about the fracture surfaces and the crack initiation and propagation modes. The high cycle fatigue strengths of plain and notched bars under torsion loading were defined at 10^7 cycles, whilst neither $\Delta K_{III,th}$ nor $\Delta K_{I,th}$ were reported in the paper.

V-notched bars made of ADI 900 ($\sigma_{UTS} \approx 900$ MPa) with $\omega = 45°$ were tested by Atzori et al. [53]. The original work does not include any information or figures about the fracture surfaces and the crack initiation and propagation modes of the plain bars, while notched bars exhibited factory roof fracture surfaces and SEM observations showed that crack initiation planes were oriented at 45° with respect to the specimen longitudinal axis. From a micromechanical point of view, crack initiation and short crack propagation were mode I-driven, therefore experimental results relevant to ADI 900 violate the assumptions underlying the FFM approaches (Eqs. (19a, b)). However, they have been included in the present analysis to check how predictions deviate from experimental results in cases outside the validity range. The high cycle fatigue strengths of plain and notched bars under torsion loading were defined at $2 \cdot 10^6$ cycles, but again neither $\Delta K_{III,th}$ nor $\Delta K_{I,th}$ were available.

Gough [86] generated experimental results by testing V-notched bars having opening angle $\omega = 55°$ and being made of several steel categories (518 MPa $\leq \sigma_{UTS} \leq$ 883 MPa). No information or figures about the fracture surfaces and the crack initiation and propagation modes were available in the work. The high cycle fatigue strengths of plain and notched bars were defined at 10^7 cycles, while neither $\Delta K_{III,th}$ nor $\Delta K_{I,th}$ were provided.

Tanaka [69] tested a carbon steel (SGV410, $\sigma_{UTS} \approx 470$ MPa) and an austenitic stainless steel (SUS316L, $\sigma_{UTS} \approx 591$ MPa) and obtained the torsion fatigue limit of V-notched bars, having opening angle $\omega = 60°$. No information or figures about the fracture surfaces of plain specimens were available, while Tanaka [69] showed that in notched bars small shear cracks initiated vertically or horizontally at the notch tip, after that they turned to cross shaped cracks driven by a tensile mode propagation. The initial flat fracture surface turned to factory-roof type as the crack extended. It was also observed that the carbon steel was more prone to shear mode crack propagation than the austenitic stainless steel: under the same stress amplitude, carbon steel is softer than austenitic one and the strain amplitude at the notch root is higher, which promotes shear crack propagation. The high cycle fatigue strengths of plain and notched bars have been defined at $2 \cdot 10^6$ cycles, while neither

$\Delta K_{III,th}$ nor $\Delta K_{I,th}$ were reported in the original paper. It is worth noting that the fatigue limits of plain materials had been derived by Tanaka in a previous work by testing hollow cylinders under torsion loading and they were provided only later in [87].

Meneghetti et al. [71] tested 90° V-notched bars made of Ti-6Al-4V ($\sigma_{UTS} \approx 1000$ MPa). Dealing with plain specimens, it was observed that multiple cracks initiated along the longitudinal direction on a plane of maximum shear stress, then crack branching occurred causing the previously parallel cracks to coalesce; eventually, the subsequent crack propagation generated almost flat fracture surfaces, where the material was completely smeared. Concerning notched bars, again multiple crack initiation points along the notch tip profile were noted: crack paths gave rise to a factory-roof fracture surface, the resulting factory-roofs were characterized by a reduced height, their peaks having been smoothed and polished during fatigue testing by the sliding contact, friction and meshing between crack surfaces. As a result, a lot of powder and debris were emanated from the notch tip. In another paper of the same authors [70], it was observed that the fracture surface of notched bars was initially flat with a depth in the range between 0.3-0.4 mm from the notch tip, after that the factory-roof morphology developed. Berto and Lazzarin [88] provided experimental torsion fatigue results generated by 90° V-notched bars and made of AISI 416 steel ($\sigma_{UTS} \approx 700$ MPa). Again, no information or figures about the fracture surfaces were available. In both cases relevant to 90° V-notched bars, the high cycle fatigue strengths of plain and notched bars under torsion loading were defined at $2 \cdot 10^6$ cycles, whilst only the high-cycle NSIF range $\Delta K_{I,A}$ obtained at $N_A = 2 \cdot 10^6$ cycles by testing 90° V-notched bars under axial fatigue loading was available in the original papers [71,88].

Material	Ref.	σ_{UTS}° (MPa)	$\Delta\sigma_0$ (MPa)	$\Delta\tau_0$ (MPa)	$\Delta K_{III,th}$ (MPa m$^{1/2}$)	$l_{th,III}$ (mm)	ω (°)	a (mm)	$2R$ (mm)	a/R	ρ (mm)	$\Delta\tau_{f,exp}$ (MPa)
Low carbon steel	[85]	500	424	362	8.46*	0.546	35	2.54	7.62	0.67	0.400	299
											0.200	241
ADI 900 or EN-GJS 800-8	[53]	900	-	574	18$^{\wedge}$	0.983	45	5.00	10.00	1.00	0.100	452
								2.00	16.00	0.25	0.100	436
0.4% C steel (normalized)	[86]	639	664	414	8.83*	0.455	55	0.51	7.62	0.13	0.005	352
3% Ni steel	[86]	518	686	410	10.12*	0.609					0.005	303
3/3.5% Ni steel	[86]	712	704	534	8.50*	0.253					0.010	367
Cr–Va steel	[86]	740	858	516	9.01*	0.305					0.011	321
3.5% NiCr steel (normal impact)	[86]	882	1080	704	8.95*	0.162					0.022	472
3.5% NiCr steel (low impact)	[86]	883	1018	648	8.72*	0.181					0.022	364
SUS316L	[69]	591	442	266^{+}	7.81*	0.861	60	2.65	10.70	0.50	0.220	215
SGV410	[69]	470	436	270^{+}	8.88*	1.081						175

Ti-6Al-4V	[71]	978	1014	894	21[#]	0.556	90	6.00	12.00	1.00	0.100	573
									13.00	0.92		451
AISI 416	[88]	700	697	474	22[#]	2.159		4.00	12.00	0.67	0.100	430
								2.00	16.00	0.25		443

° equivalent to σ_c as defined under static loading

* estimated by Eq. (23) with α=1, where $\Delta K_{I,th}$ has first been estimated from Eq. (25)

^ estimated by Eq. (23) with α=1, where $\Delta K_{I,th}$ has first been estimated from Eq. (26) with α_R=2 having $\Delta K_{I,th,R=0.1}$ from [84].

+ experimental results derived by hollow cylinders or solid bars (elastic-plastic FE analysis) and reported in [87]

[#] estimated by Eq. (23) α=1, where $\Delta K_{I,th}$ has been derived by assuming the sharp V-notch case with ω = 90° as equivalent to the crack case under mode I loading

Table 2. Experimental fatigue results under torsion loading generated by notched bars (Fig. 6) re-analysed according to the FFM approaches Eqs. (19a,b). R_L represents the loading ratio and it is equal to -1 in all cases. For details on the experimental procedures and the scatter of data, see the corresponding references.

Fatigue limit predictions are presented in Figs. 8-12, together with experimental results related V-notched bars, having different notch depths and opening angles, and being made of several metallic materials, whose properties are reported in Table 2. Observing that FFM approaches underly many engineering assumptions as described in Section 4.1, and that $\Delta K_{III,th}$ is estimated through empirical equations, i.e. Eqs. (23) and (25) in most of the considered cases, the matching between FFM fracture strength and experimental data can be considered satisfactory. In this case, FFM-PS provides the most accurate predictions, whereas FFM-AS, as usual, reveals more conservative. All in all, 16 experimental fatigue limits have been compared with the FFM-based predictions and it results that FFM-PS and FFM-AS provide predictions on the safe side in 11 and 13 out of 16 cases, respectively. Finally, it is worth noting that: i) for low carbon steel, the radius ρ = 0.4 mm is not small compared to the threshold length $l_{th,III}$: FFM predictions thus underestimate the corresponding recorded data (Fig. 8); even in the case of ADI 900, which violates the present FFM assumptions, theoretical results are in pretty good agreement with experimental ones (Fig. 9).

Fig. 8. V-notched bars under torsion loading, ω = 35°: FFM fatigue limits and experimental data from [85].

Fig. 9. V-notched bars under torsion loading, ω = 45°: FFM fatigue limits and experimental data from [53].

Fig. 10. V-notched bars under torsion loading, ω = 55°: FFM fatigue limits and experimental data from [86].

Fig. 11. V-notched bars under torsion loading, ω = 60°: FFM fatigue limits and experimental data from [69].

Fig. 12. V-notched bars under torsion loading, ω = 90°: FFM fatigue limits and experimental data from [71,88].

5. Conclusions

The coupled FFM approach was applied to assess brittle crack initiation in sharp V-notched structures under mode III loading conditions. It was supposed that failure is shear-stress governed and that the fracture propagates along the notch bisector plane. These simplifying assumptions were discussed both in the static and the fatigue regimes by considering a large variety of experimental results on cylindrical structures, and focusing on the estimation of the material properties necessary to implement the criterion. On one hand, although the present FFM approach provides satisfactory predictions, the case of static fracture should be assessed by means of a different analysis, considering friction and plasticity and, eventually, a different (tensile) failure mechanism for very brittle materials. On the other hand, despite the adopted hypotheses (Section 4) are simplistic to rigorously account for all the physical phenomena which occur in the fatigue process zone for metallic materials, the model reveals reliable and promising for V-notched structures under cyclic mode III loading conditions. Note that the estimation of the mode III threshold value $\Delta K_{III,th}$ still remains an 'open question': our choice to set $\alpha = 1$ in the simplifying relationship expressed through Eq. (23) leads to conservative FFM predictions.

References

[1] Leguillon D. Strength or toughness? A criterion for crack onset at a notch. Eur J Mech - A/Solids 2002;21:61–72. https://doi.org/10.1016/S0997-7538(01)01184-6.

[2] Cornetti P, Pugno N, Carpinteri A, Taylor D. Finite fracture mechanics: A coupled stress and energy failure criterion. Eng Fract Mech 2006;73:2021–33. https://doi.org/10.1016/j.engfracmech.2006.03.010.

[3] Seweryn A. A non-local stress and strain energy release rate mixed mode fracture initiation and propagation criteria. Eng Fract Mech 1998;59:737–60. https://doi.org/10.1016/S0013-7944(97)00175-6.

[4] Taylor D. Geometrical effects in fatigue: a unifying theoretical model. Int J Fatigue 1999;21:413–20. https://doi.org/10.1016/S0142-1123(99)00007-9.

[5] Taylor D. The Theory of Critical Distances. A New Perspective in Fracture Mechanics. London: Elsevier; 2007. https://doi.org/10.1016/B978-0-08-044478-9.X5000-5.

[6] Pugno NM, Ruoff RS. Quantized fracture mechanics. Philos Mag 2004;84:2829–45. https://doi.org/10.1080/14786430412331280382.

[7] Carpinteri A, Cornetti P, Pugno N, Sapora A, Taylor D. A finite fracture mechanics approach to structures with sharp V-notches. Eng Fract Mech 2008;75:1736–52. https://doi.org/10.1016/j.engfracmech.2007.04.010.

[8] Lazzarin P, Campagnolo A, Berto F. A comparison among some recent energy- and stress-based criteria for the fracture assessment of sharp V-notched components under Mode I loading. Theor Appl Fract Mech 2014;71:21–30. https://doi.org/10.1016/j.tafmec.2014.03.001.

[9] Sapora A, Cornetti P, Carpinteri A. V-notched elements under mode II loading conditions.

Struct Eng Mech 2014;49:499–508. https://doi.org/10.12989/sem.2014.49.4.499.
[10] Campagnolo A, Berto F, Leguillon D. Fracture assessment of sharp V-notched components under Mode II loading: a comparison among some recent criteria. Theor Appl Fract Mech 2016;85:Accepted. https://doi.org/10.1016/j.tafmec.2016.02.001.
[11] Yosibash Z, Priel E, Leguillon D. A failure criterion for brittle elastic materials under mixed-mode loading. Int J Fract 2006;141:291–312. https://doi.org/10.1007/s10704-006-0083-6.
[12] Priel E, Bussiba A, Gilad I, Yosibash Z. Mixed mode failure criteria for brittle elastic V-notched structures. Int J Fract 2007;144:247–65. https://doi.org/10.1007/s10704-007-9098-x.
[13] Sapora A, Cornetti P, Carpinteri A. A Finite Fracture Mechanics approach to V-notched elements subjected to mixed-mode loading. Eng Fract Mech 2013;97:216–26. https://doi.org/10.1016/j.engfracmech.2012.11.006.
[14] Cornetti P, Sapora A, Carpinteri A. T-stress effects on crack kinking in Finite Fracture Mechanics. Eng Fract Mech 2014;132:169–76. https://doi.org/10.1016/j.engfracmech.2014.10.011.
[15] Mittelman B, Yosibash Z. Energy release rate cannot predict crack initiation orientation in domains with a sharp V-notch under mode III loading. Eng Fract Mech 2015;141:230–41. https://doi.org/10.1016/j.engfracmech.2015.05.008.
[16] Yosibash Z, Mittelman B. A 3-D failure initiation criterion from a sharp V-notch edge in elastic brittle structures. Eur J Mech - A/Solids 2016;60:70–94. https://doi.org/10.1016/j.euromechsol.2016.06.003.
[17] Doitrand A, Leguillon D. Numerical modeling of the nucleation of facets ahead of a primary crack under mode I + III loading. Int J Fract 2018;213:37–50. https://doi.org/10.1007/s10704-018-0305-8.
[18] Sapora A, Cornetti P, Campagnolo A, Meneghetti G. Fatigue limit: Crack and notch sensitivity by Finite Fracture Mechanics. Theor Appl Fract Mech 2020;105:102407. https://doi.org/10.1016/j.tafmec.2019.102407.
[19] Sapora A, Cornetti P, Campagnolo A, Meneghetti G. Mode I fatigue limit of notched structures: A deeper insight into Finite Fracture Mechanics. Int J Fract 2021;227:1–13. https://doi.org/10.1007/s10704-020-00488-6.
[20] Cornetti P, Sapora A, Carpinteri A. Short cracks and V-notches: Finite Fracture Mechanics vs. Cohesive Crack Model. Eng Fract Mech 2016;168:2–12. https://doi.org/10.1016/j.engfracmech.2015.12.016.
[21] Doitrand A, Estevez R, Leguillon D. Comparison between cohesive zone and coupled criterion modeling of crack initiation in rhombus hole specimens under quasi-static compression. Theor Appl Fract Mech 2019;99:51–9. https://doi.org/10.1016/j.tafmec.2018.11.007.
[22] Cornetti P, Muñoz-Reja M, Sapora A, Carpinteri A. Finite fracture mechanics and cohesive crack model: Weight functions vs. cohesive laws. Int J Solids Struct 2019;156–157:126–36. https://doi.org/10.1016/j.ijsolstr.2018.08.003.
[23] Qian J, Hasebe N. Property of eigenvalues and eigenfunctions for an interface V-notch in antiplane elasticity. Eng Fract Mech 1997;56:729–34. https://doi.org/10.1016/S0013-7944(97)00004-0.
[24] Zappalorto M, Lazzarin P, Berto F. Elastic notch stress intensity factors for sharply V-notched rounded bars under torsion. Eng Fract Mech 2009;76:439–53. https://doi.org/10.1016/j.engfracmech.2008.11.008.
[25] Duan J, Li X, Lei Y. A note on stress intensity factors for a crack emanating from a sharp V-notch. Eng Fract Mech 2012;90:180–7. https://doi.org/10.1016/j.engfracmech.2012.04.023.
[26] Salviato M, Zappalorto M, Maragoni L. Exact solution for the mode III stress fields ahead of cracks initiated at sharp notch tips. Eur J Mech - A/Solids 2018;72:88–96. https://doi.org/10.1016/j.euromechsol.2018.04.014.
[27] Zappalorto M, Salviato M, Maragoni L. Analytical study on the mode III stress fields due to blunt notches with cracks. Fatigue Fract Eng Mater Struct 2019;42:612–26.

https://doi.org/10.1111/ffe.12936.
[28] Atzori B, Lazzarin P, Meneghetti G. A unified treatment of the mode I fatigue limit of components containing notches or defects. Int J Fract 2005;133:61–87. https://doi.org/10.1007/s10704-005-2183-0.
[29] Richard HA, Eberlein A, Kullmer G. Concepts and experimental results for stable and unstable crack growth under 3D-mixed-mode-loadings. Eng Fract Mech 2017;174:10–20. https://doi.org/10.1016/j.engfracmech.2016.12.005.
[30] Sapora A, Cornetti P, Carpinteri A, Firrao D. An improved Finite Fracture Mechanics approach to blunt V-notch brittle fracture mechanics: Experimental verification on ceramic, metallic, and plastic materials. Theor Appl Fract Mech 2015;78:20–4. https://doi.org/10.1016/j.tafmec.2015.04.004.
[31] Santus C, Berto F, Pedranz M, Benedetti M. Mode III critical distance determination with optimized V-notched specimen under torsional fatigue and size effects on the inverse search probability distribution. Int J Fatigue 2021;151:106351. https://doi.org/10.1016/j.ijfatigue.2021.106351.
[32] Liu S, Chao YJ, Zhu X. Tensile-shear transition in mixed mode I/III fracture. Int J Solids Struct 2004;41:6147–72. https://doi.org/10.1016/j.ijsolstr.2004.04.044.
[33] Lazarus V, Buchholz F-G, Fulland M, Wiebesiek J. Comparison of predictions by mode II or mode III criteria on crack front twisting in three or four point bending experiments. Int J Fract 2008;153:141–51. https://doi.org/10.1007/s10704-008-9307-2.
[34] Lazarus V, Leblond J-B, Mouchrif S-E. Crack front rotation and segmentation in mixed mode I+III or I+II+III. Part II: Comparison with experiments. J Mech Phys Solids 2001;49:1421–43. https://doi.org/10.1016/S0022-5096(01)00008-4.
[35] Lazarus V, Leblond J-B, Mouchrif S-E. Crack front rotation and segmentation in mixed mode I+III or I+II+III. Part I: Calculation of stress intensity factors. J Mech Phys Solids 2001;49:1399–420. https://doi.org/10.1016/S0022-5096(01)00007-2.
[36] Pham KH, Ravi-Chandar K. Further examination of the criterion for crack initiation under mixed-mode I+III loading. Int J Fract 2014;189:121–38. https://doi.org/10.1007/s10704-014-9966-0.
[37] Pham KH, Ravi-Chandar K. On the growth of cracks under mixed-mode I + III loading. Int J Fract 2016;199:105–34. https://doi.org/10.1007/s10704-016-0098-6.
[38] Leblond J-B, Karma A, Lazarus V. Theoretical analysis of crack front instability in mode I+III. J Mech Phys Solids 2011;59:1872–87. https://doi.org/10.1016/j.jmps.2011.05.011.
[39] Leblond J-B, Lazarus V, Karma A. Multiscale cohesive zone model for propagation of segmented crack fronts in mode I+III fracture. Int J Fract 2015;191:167–89. https://doi.org/10.1007/s10704-015-0001-x.
[40] Zehnder AT, Zella NK. Spiral to flat fracture transition for notched rods under torsional loading. Int J Fract 2015;195:87–92. https://doi.org/10.1007/s10704-015-0049-7.
[41] Berto F, Lazzarin P, Ayatollahi MR. Brittle fracture of sharp and blunt V-notches in isostatic graphite under torsion loading. Carbon N Y 2012;50:1942–52. https://doi.org/10.1016/j.carbon.2011.12.045.
[42] Berto F, Elices M, Lazzarin P, Zappalorto M. Fracture behaviour of notched round bars made of PMMA subjected to torsion at room temperature. Eng Fract Mech 2012;90:143–60. https://doi.org/10.1016/j.engfracmech.2012.05.001.
[43] Berto F, Cendon DAA, Lazzarin P, Elices M. Fracture behaviour of notched round bars made of PMMA subjected to torsion at −60°C. Eng Fract Mech 2013;102:271–87. https://doi.org/10.1016/j.engfracmech.2013.02.011.
[44] Berto F, Campagnolo A, Ayatollahi MRR. Brittle Fracture of Rounded V-Notches in Isostatic Graphite under Static Multiaxial Loading. Phys Mesomech 2015;18:283–97. https://doi.org/10.1134/S1029959915040025.
[45] Susmel L, Taylor D. On the use of the Theory of Critical Distances to predict static failures in

ductile metallic materials containing different geometrical features. Eng Fract Mech 2008;75:4410–21. https://doi.org/10.1016/j.engfracmech.2008.04.018.
[46] Madrazo V, Cicero S, Carrascal IA. On the Point Method and the Line Method notch effect predictions in Al7075-T651. Eng Fract Mech 2012;79:363–79. https://doi.org/10.1016/j.engfracmech.2011.11.017.
[47] Torabi AR. Estimation of tensile load-bearing capacity of ductile metallic materials weakened by a V-notch: The equivalent material concept. Mater Sci Eng A 2012;536:249–55. https://doi.org/10.1016/j.msea.2012.01.007.
[48] Sapora A, Firrao D. Finite fracture mechanics predictions on the apparent fracture toughness of as-quenched Charpy V-type AISI 4340 steel specimens. Fatigue Fract Eng Mater Struct 2017;40:949–58. https://doi.org/10.1111/ffe.12555.
[49] Torabi AR, Berto F, Sapora A. Finite Fracture Mechanics Assessment in Moderate and Large Scale Yielding Regimes. Metals (Basel) 2019;9:602. https://doi.org/10.3390/met9050602.
[50] Ayatollahi MR, Saboori B. A new fixture for fracture tests under mixed mode I/III loading. Eur J Mech - A/Solids 2015;51:67–76. https://doi.org/10.1016/j.euromechsol.2014.09.012.
[51] Torabi AR, Saboori B, Mohammadian SK, Ayatollahi MR. Brittle failure of PMMA in the presence of blunt V-notches under combined tension-tear loading: Experiments and stress-based theories. Polym Test 2018;72:94–109. https://doi.org/10.1016/j.polymertesting.2018.10.002.
[52] Atzori B, Meneghetti G. Notch and Defect Sensitivity of Adi in Torsional Fatigue. Fract. Nano Eng. Mater. Struct., Dordrecht: Springer Netherlands; n.d., p. 201–2. https://doi.org/10.1007/1-4020-4972-2_98.
[53] Atzori B, Meneghetti G. Notch and Defect Sensitivity of ADI in Torsional Fatigue. Proc. 16th Eur. Conf. Fract. ECF 16, Alexandropoulis, Greece: 2006.
[54] Susmel L, Taylor D. A simplified approach to apply the theory of critical distances to notched components under torsional fatigue loading. Int J Fatigue 2006;28:417–30. https://doi.org/10.1016/j.ijfatigue.2005.07.035.
[55] Atzori B, Zappalorto M, Berto F. A theoretical treatise for notch and defect sensitivity under torsion. Mech Res Commun 2010;37:173–6. https://doi.org/10.1016/j.mechrescom.2009.12.005.
[56] Susmel L, Taylor D. The Theory of Critical Distances to estimate finite lifetime of notched components subjected to constant and variable amplitude torsional loading. Eng Fract Mech 2013;98:64–79. https://doi.org/10.1016/j.engfracmech.2012.12.007.
[57] Socie D, Bannantine J. Bulk deformation fatigue damage models. Mater Sci Eng A 1988;103:3–13. https://doi.org/10.1016/0025-5416(88)90546-0.
[58] Marquis G, Socie D. Long-life torsion fatigue with normal mean stresses. Fatigue Fract Eng Mater Struct 2000;23:293–300. https://doi.org/10.1046/j.1460-2695.2000.00291.x.
[59] Murakami Y, Takahashi K. Torsional fatigue of a medium carbon steel containing an initial small surface crack introduced by tension-compression fatigue: crack branching, non-propagation and fatigue limit. Fatigue Fract Eng Mater Struct 1998;21:1473–84. https://doi.org/10.1046/j.1460-2695.1998.00128.x.
[60] Atzori B, Lazzarin P, Quaresimin M. Fatigue Behaviour of a Sharply Notched Carbon Steel under Torsion. Proc. Fatigue Crack Paths Int. Conf., 2003.
[61] Makabe C, Socie DF. Crack growth mechanism in precracked torsional fatigue specimens. Fatigue Fract Eng Mater Struct 2001;24:607–15. https://doi.org/10.1046/j.1460-2695.2001.00430.x.
[62] Tschegg EK. A contribution to mode III fatigue crack propagation. Mater Sci Eng 1982;54:127–36. https://doi.org/10.1016/0025-5416(82)90037-4.
[63] Ritchie RO, McClintock FA, Nayeb-Hashemi H, Ritter MA. Mode III fatigue crack propagation in low alloy steel. Metall Trans A 1982;13:101–10. https://doi.org/10.1007/BF02642420.

[64] Tschegg EK. Mode III and Mode I fatigue crack propagation behaviour under torsional loading. J Mater Sci 1983;18:1604–14. https://doi.org/10.1007/BF00542053.
[65] Hellier AK, Corderoy DJH, McGirr MB. Some observations on mode III fatigue thresholds. Int J Fract 1985;29:R45–8. https://doi.org/10.1007/BF00125475.
[66] Yates JR, Miller KJ. Mixed mode (I+III) fatigue thresholds in a forging steel. Fatigue Fract Eng Mater Struct 1989;12:259–70. https://doi.org/10.1111/j.1460-2695.1989.tb00532.x.
[67] Yu H, Tanaka K, Akiniwa Y. Estimation of torsional fatigue strength of medium carbon steel bars with a circumferential crack by the cyclic resistance-curve method. Fatigue Fract Eng Mater Struct 1998;21:1067–76. https://doi.org/10.1046/j.1460-2695.1998.00105.x.
[68] Murakami Y, Takahashi K, Kusumoto R. Threshold and growth mechanism of fatigue cracks under mode II and III loadings. Fatigue Fract Eng Mater Struct 2003;26:523–31. https://doi.org/10.1046/j.1460-2695.2003.00644.x.
[69] Tanaka K. Crack initiation and propagation in torsional fatigue of circumferentially notched steel bars. Int J Fatigue 2014;58:114–25. https://doi.org/10.1016/j.ijfatigue.2013.01.002.
[70] Campagnolo A, Meneghetti G, Berto F, Tanaka K. Calibration of the potential drop method by means of electric FE analyses and experimental validation for a range of crack shapes. Fatigue Fract Eng Mater Struct 2018;41:1–16. https://doi.org/10.1111/ffe.12856.
[71] Meneghetti G, Campagnolo A, Berto F, Tanaka K. Notched Ti-6Al-4V titanium bars under multiaxial fatigue: Synthesis of crack initiation life based on the averaged strain energy density. Theor Appl Fract Mech 2018;96:509–33. https://doi.org/10.1016/j.tafmec.2018.06.010.
[72] Berto F, Lazzarin P, Yates JR. Multiaxial fatigue of V-notched steel specimens: A non-conventional application of the local energy method. Fatigue Fract Eng Mater Struct 2011;34:921–43. https://doi.org/10.1111/j.1460-2695.2011.01585.x.
[73] Pokluda J, Pippan R. Can pure mode III fatigue loading contribute to crack propagation in metallic materials? Fatigue Fract Eng Mater Struct 2008;28:179–85. https://doi.org/10.1111/j.1460-2695.2004.00843.x.
[74] Pokluda J, Pippan R, Slàmecka K, Kolednik O. Fatigue crack growth in metals under pure mode III: reality or fiction? In: Carpinteri A, Pook LP, editors. Fatigue crack paths. Parma: University of Parma; 2003. p. 92–7. In: Carpinteri A PL, editor. Proceeding of the Fatigue crack paths, Parma: 2003, p. 92–7.
[75] Tanaka K, Hashimoto A, Narita J, Egami N. Fatigue life of circumferentially notched bars of austenitic stainless steel under cyclic torsion with and without static tension. J Soc Mater Sci Jpn 2009;58:1044–1050.
[76] Okano T, Hisamatsu N. Effect of notch of torsional fatigue property of pure titanium. Proc 31 Symp Fatigue, Soc Mater Sci Japan 2012;31:129–133.
[77] Endo M, Murakami Y. Effects of an Artificial Small Defect on Torsional Fatigue Strength of Steels. J Eng Mater Technol 1987;109:124–9. https://doi.org/10.1115/1.3225951.
[78] ASTM. ASTM Standard E647 - 15e1, Standard Test Method for Measurement of Fatigue Crack Growth Rates 2015. https://doi.org/10.1520/E0647-15E01.2.
[79] Pook LP, Sharples JK. The mode III fatigue crack growth threshold for mild steel. Int J Fract 1979;15:R223–6. https://doi.org/10.1007/BF00019933.
[80] Pook LP. Mixed-mode fatigue crack growth thresholds: A personal historical review of work at the National Engineering Laboratory, 1975–1989. Eng Fract Mech 2018;187:115–41. https://doi.org/10.1016/j.engfracmech.2017.10.028.
[81] Beretta S, Murakami Y. SIF and threshold for small cracks at small notches under torsion. Fatigue Fract Eng Mater Struct 2000;23:97–104. https://doi.org/10.1046/j.1460-2695.2000.00260.x.
[82] Richard HA, Schramm B, Schirmeisen N-H. Cracks on Mixed Mode loading – Theories, experiments, simulations. Int J Fatigue 2014;62:93–103. https://doi.org/10.1016/j.ijfatigue.2013.06.019.

[83] Taylor D. Fatigue thresholds. Butterworths & co; 1989.
[84] Atzori B, Meneghetti G, Susmel L. Material fatigue properties for assessing mechanical components weakened by notches and defects. Fatigue Fract Eng Mater Struct 2008;28:83–97. https://doi.org/10.1111/j.1460-2695.2004.00862.x.
[85] Quilafku G, Kadi N, Dobranski J, Azari Z, Gjonaj M, Pluvinage G. Fatigue of specimens subjected to combined loading. Role of hydrostatic pressure. Int J Fatigue 2001;23:689–701. https://doi.org/10.1016/S0142-1123(01)00030-5.
[86] Gough HJ. Engineering Steels under Combined Cyclic and Static Stresses. Proc Inst Mech Eng 1949;160:417–40. https://doi.org/10.1243/PIME_PROC_1949_160_040_02.
[87] Campagnolo A, Meneghetti G, Berto F, Tanaka K. Crack initiation life in notched steel bars under torsional fatigue: Synthesis based on the averaged strain energy density approach. Int J Fatigue 2017;100:563–74. https://doi.org/10.1016/j.ijfatigue.2016.12.022.
[88] Berto F, Lazzarin P. Fatigue strength of structural components under multi-axial loading in terms of local energy density averaged on a control volume. Int J Fatigue 2011;33:1055–65. https://doi.org/10.1016/j.ijfatigue.2010.11.019.

Appendix

The following are the shape functions calculated by Zappalorto et al. [24] in accordance with our NSIF notation (2), see Eq. (16):

$$\begin{aligned} k_3(30°,\psi) &= 5.2125\cdot10^{-4}\psi^{-2} - 2.6341\cdot10^{-2}\psi^{-1} + 0.7454 \\ k_3(60°,\psi) &= 3.6731\cdot10^{-4}\psi^{-2} - 2.1861\cdot10^{-2}\psi^{-1} + 0.8064 \\ k_3(90°,\psi) &= 1.9675\cdot10^{-4}\psi^{-2} - 1.5992\cdot10^{-2}\psi^{-1} + 0.8718 \\ k_3(120°,\psi) &= 0.1134\cdot10^{-4}\psi^{-2} - 0.7964\cdot10^{-2}\psi^{-1} + 0.9274 \end{aligned} \qquad \text{(A1)}$$

where $\psi = a/R$, $1/20 \le \psi \le 1$.

Figure 1

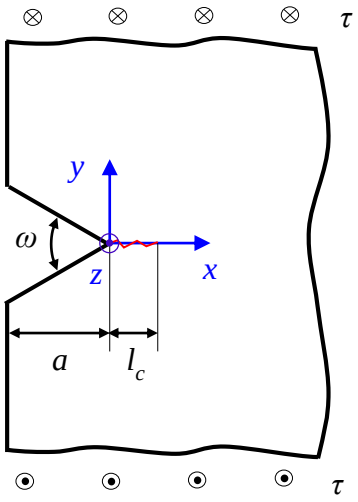

Figure 2

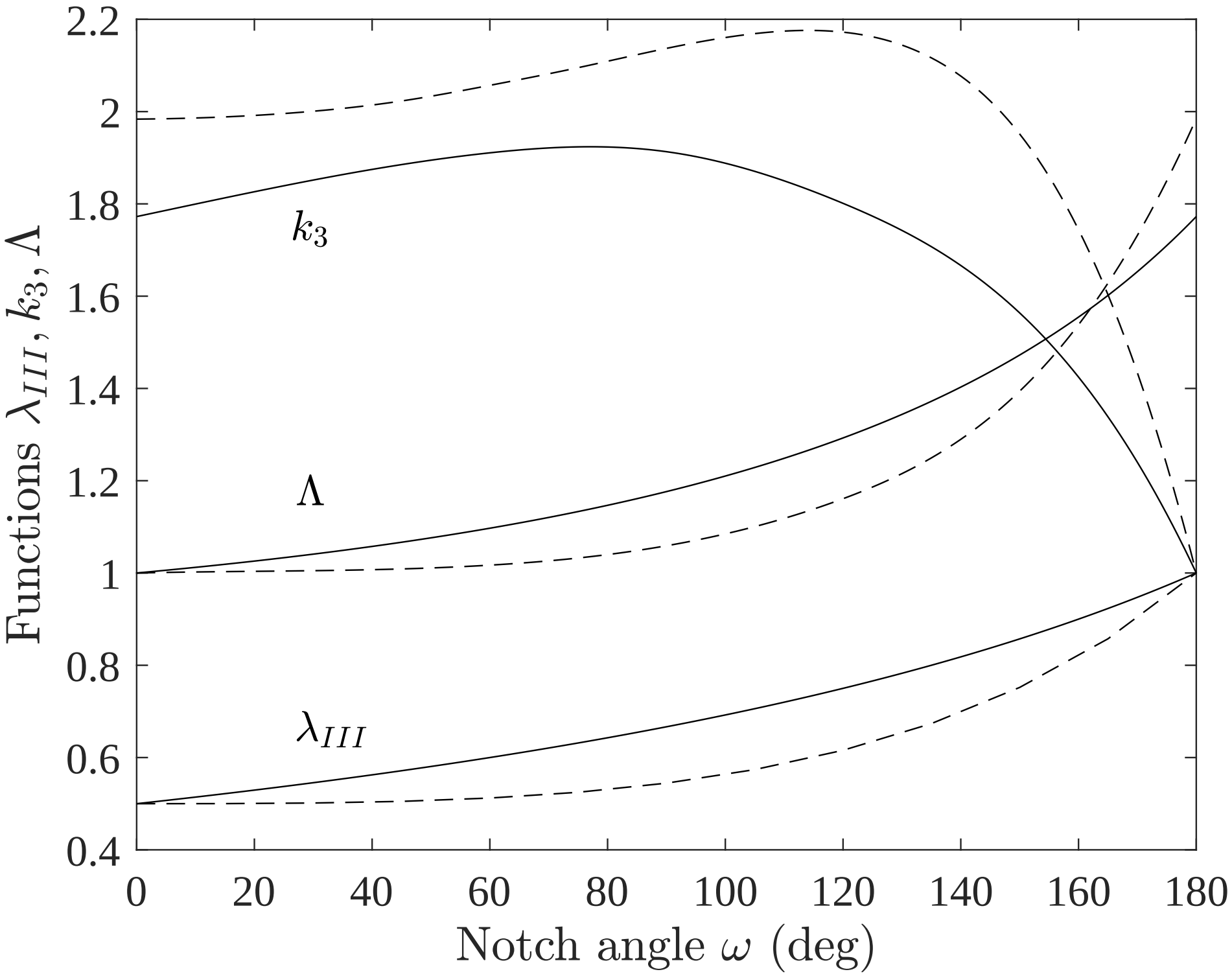

Figure 3

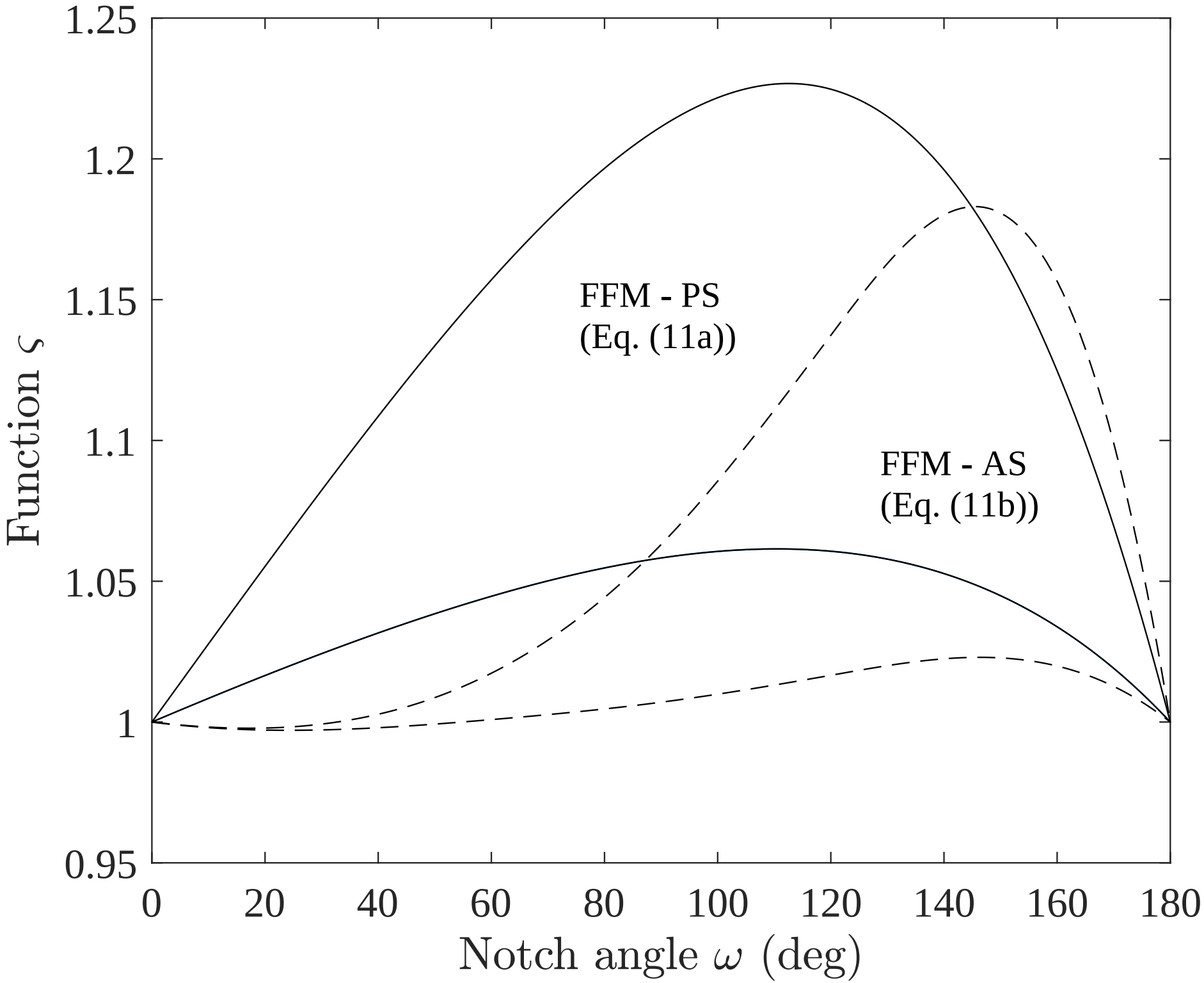

Figure 4

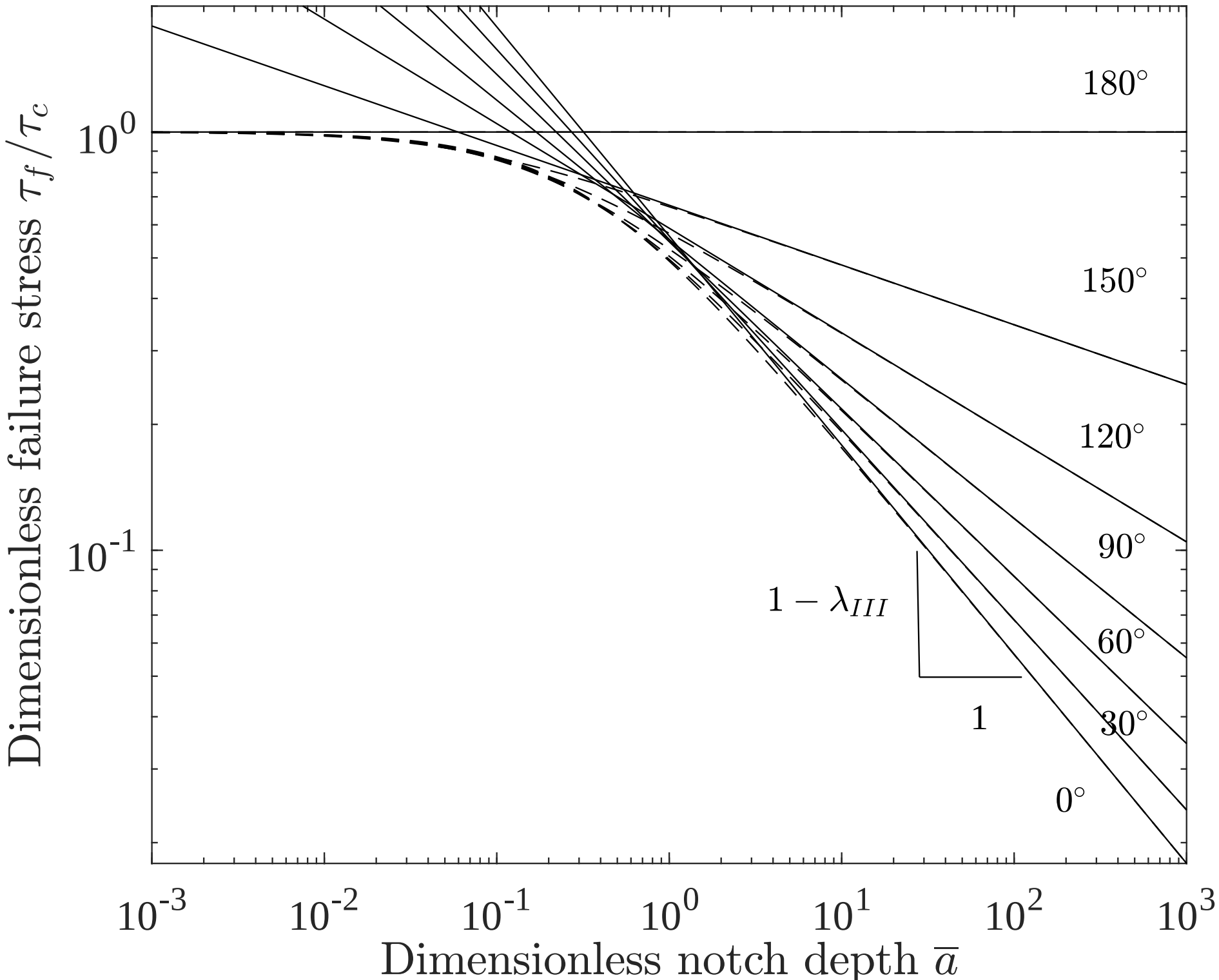

Figure 5

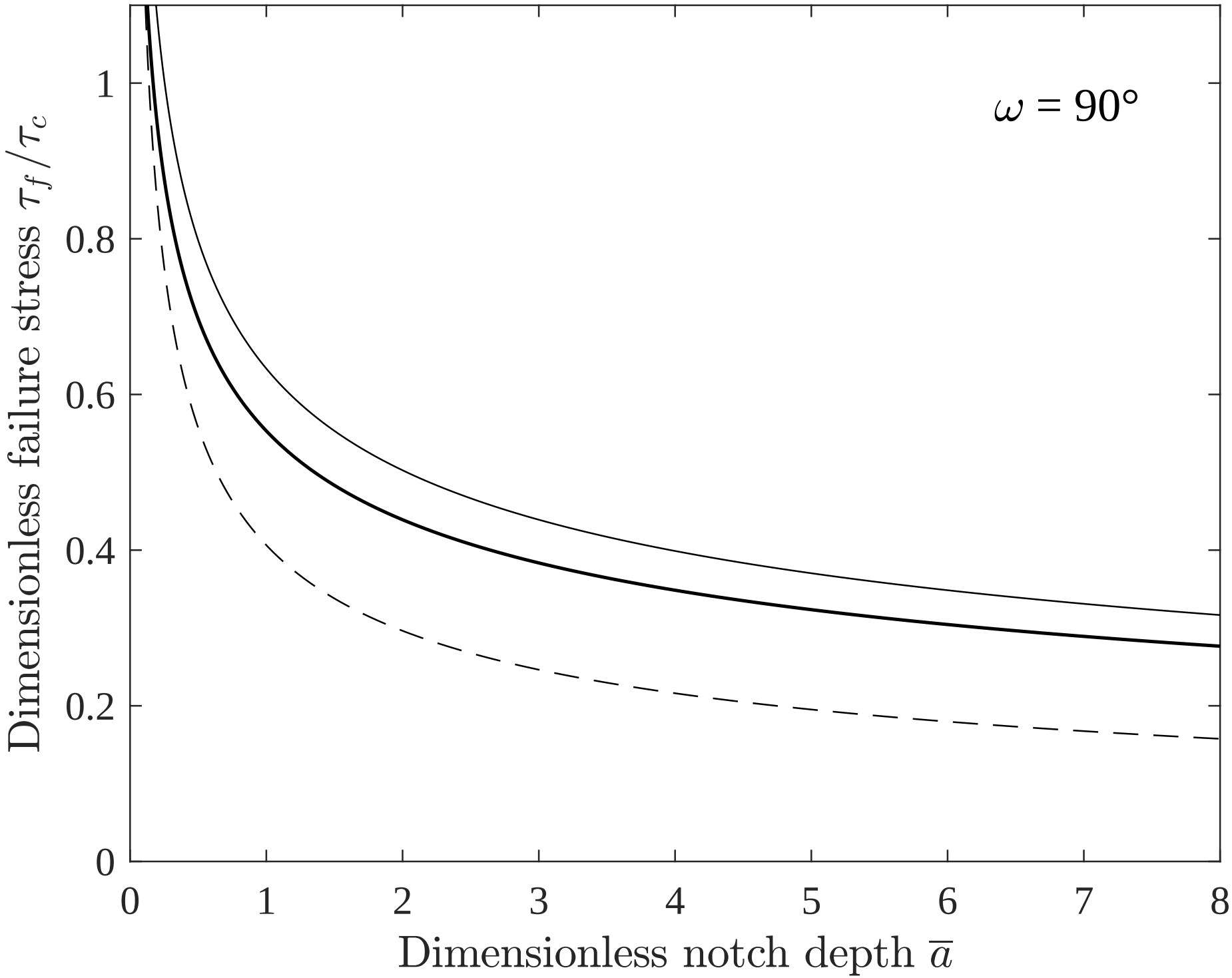

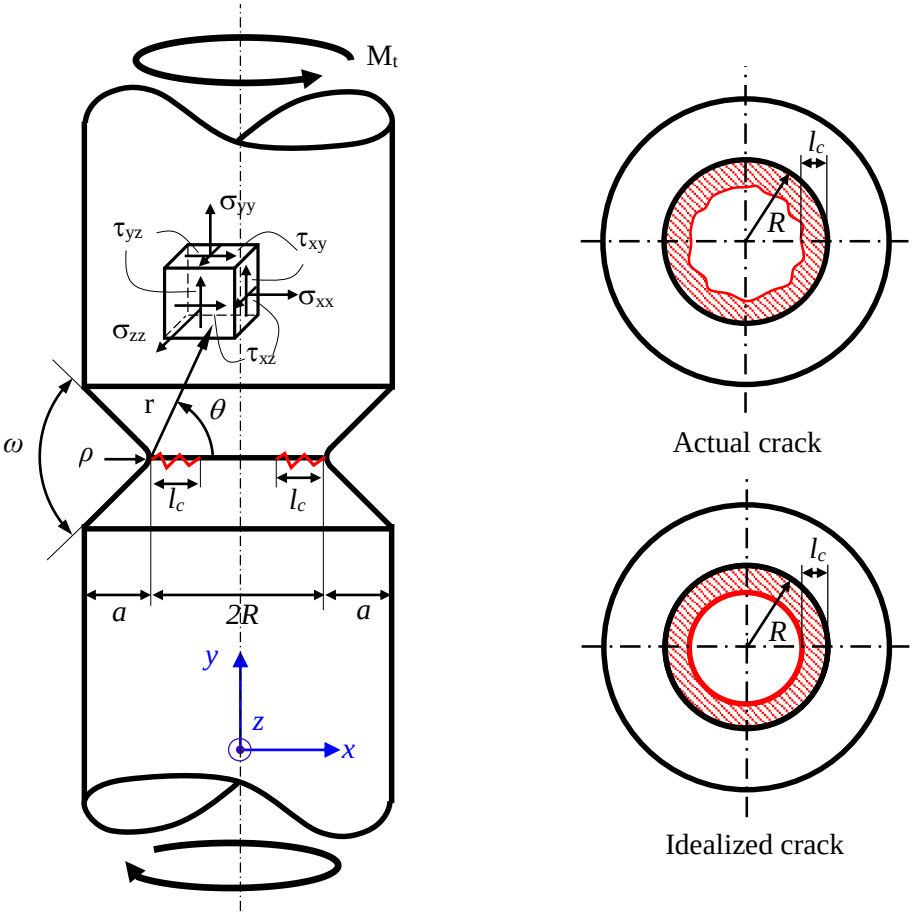

Figure 7a

Click here to access/download;Figure;Fig. 7a.eps

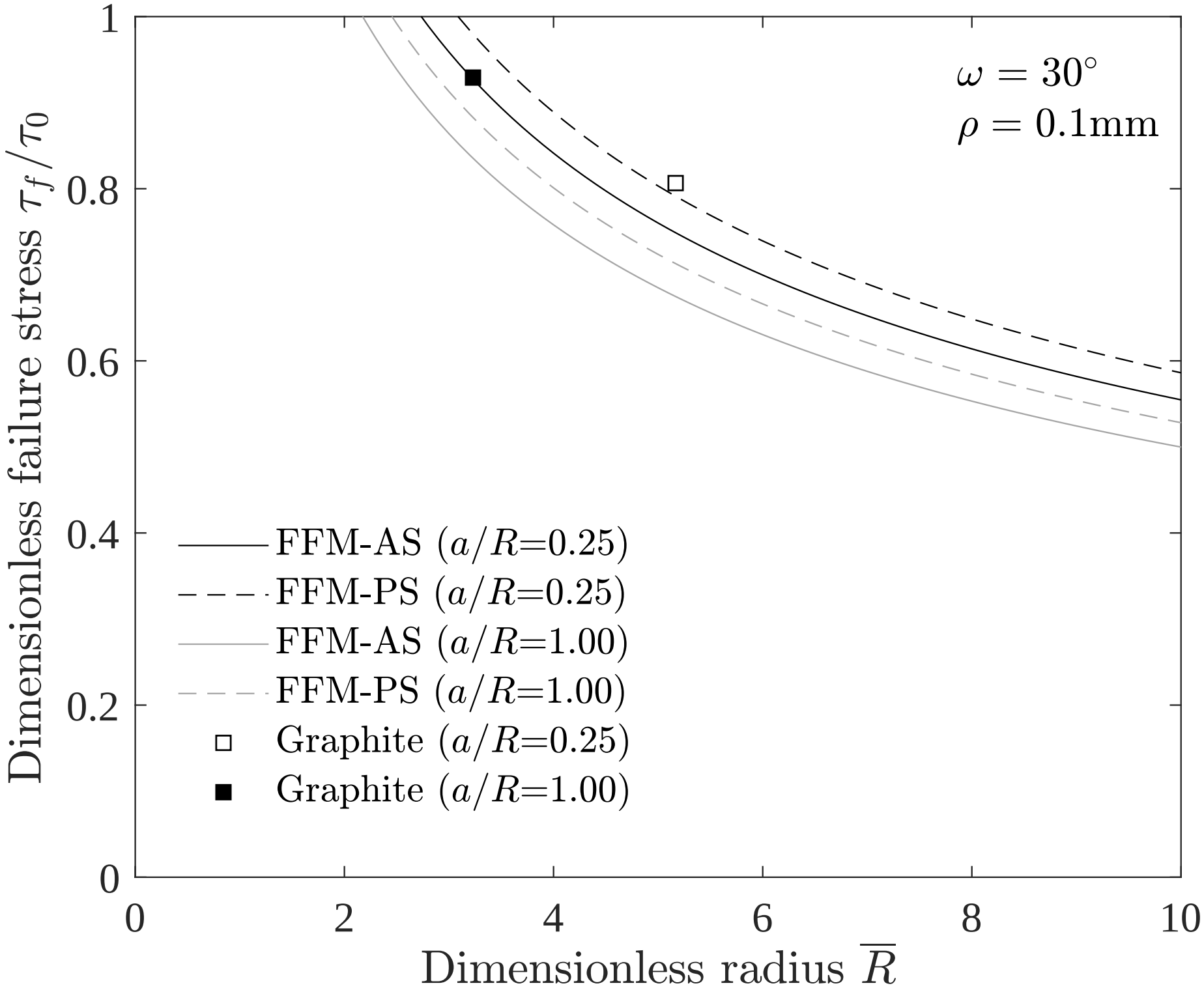

Figure 7b

Click here to access/download;Figure;Fig. 7b.eps

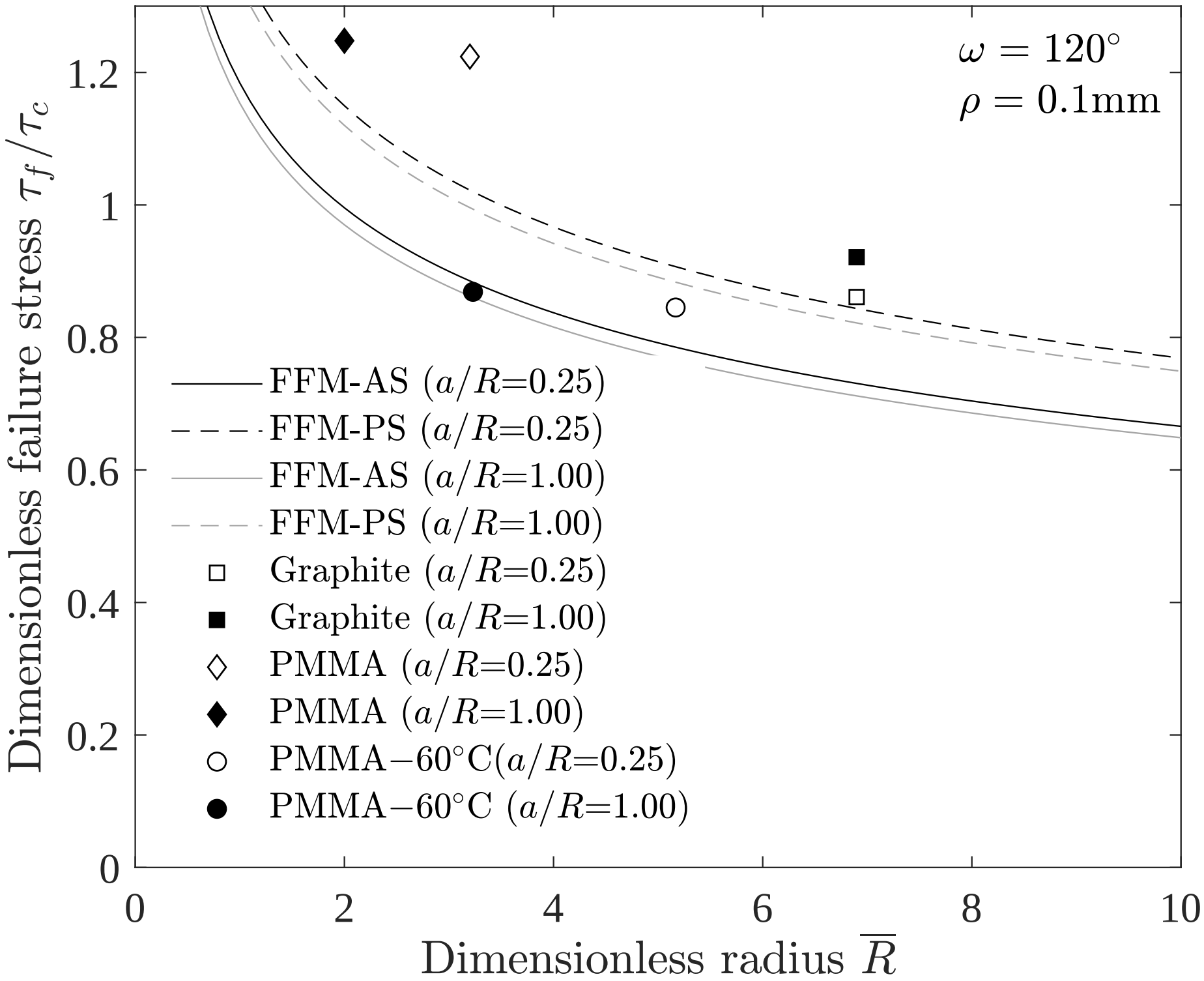

Figure 8

Click here to access/download;Figure;Fig. 8.eps

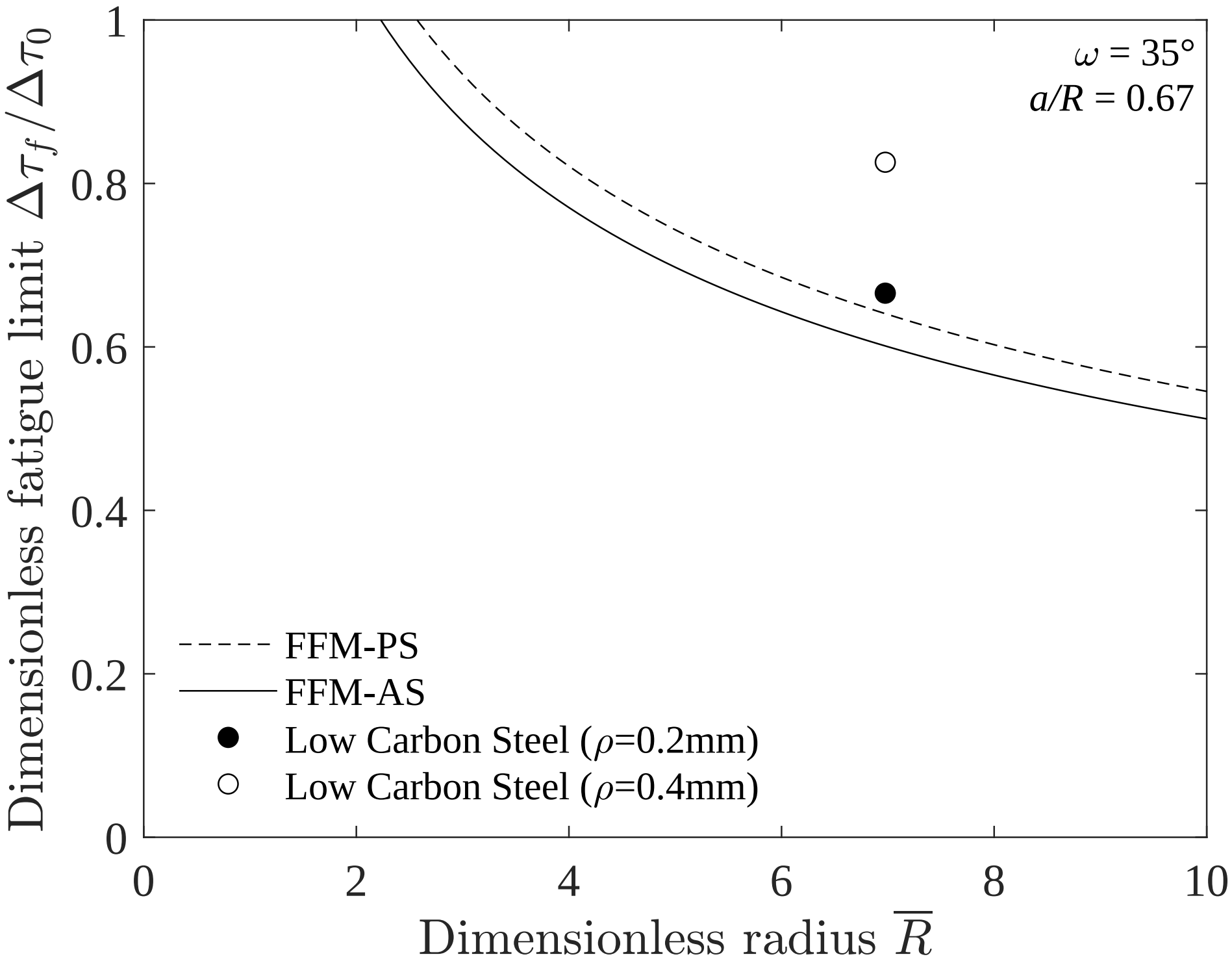

Figure 9

Click here to access/download;Figure;Fig. 9.eps

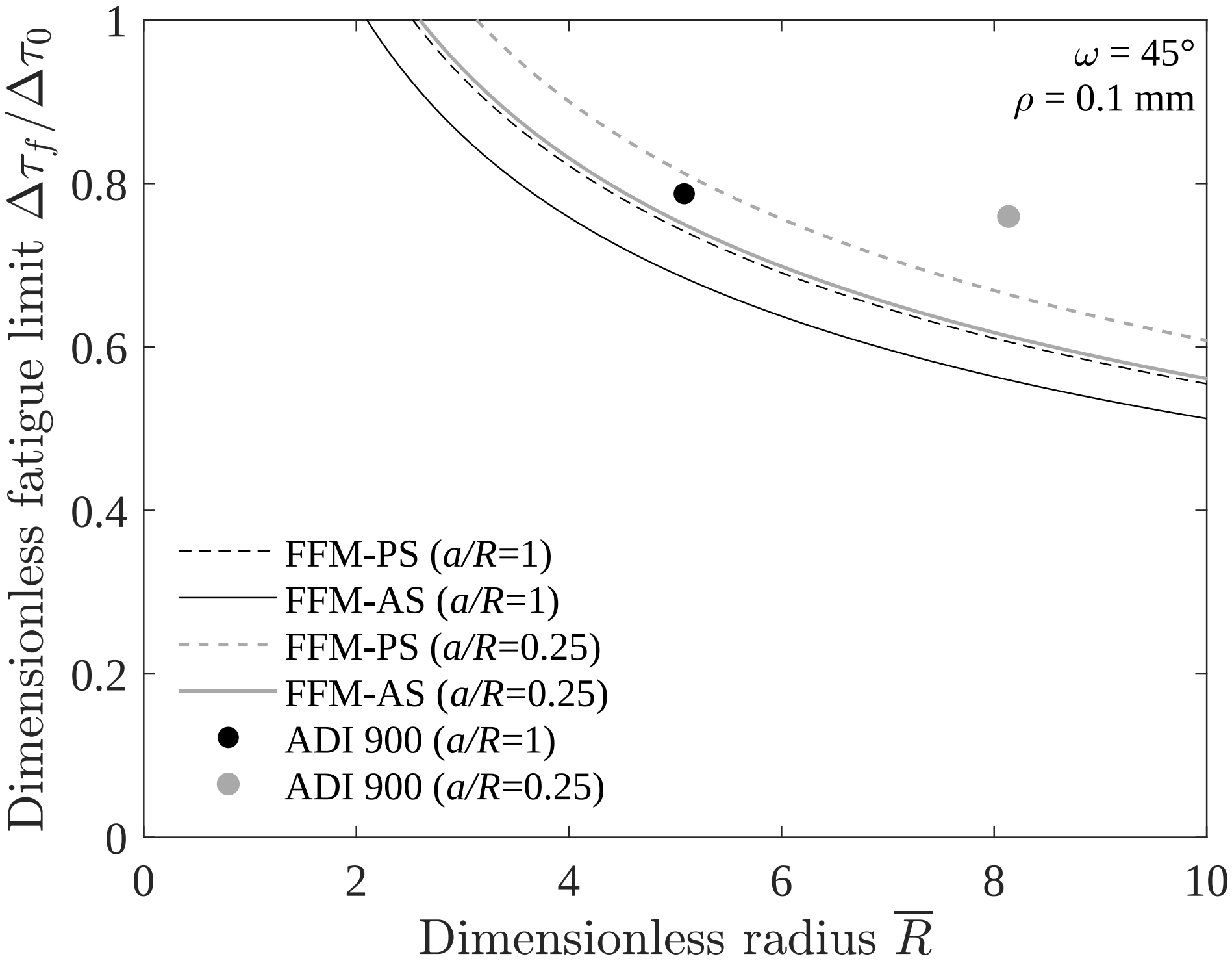

Figure 10

Click here to access/download;Figure;Fig. 10.eps

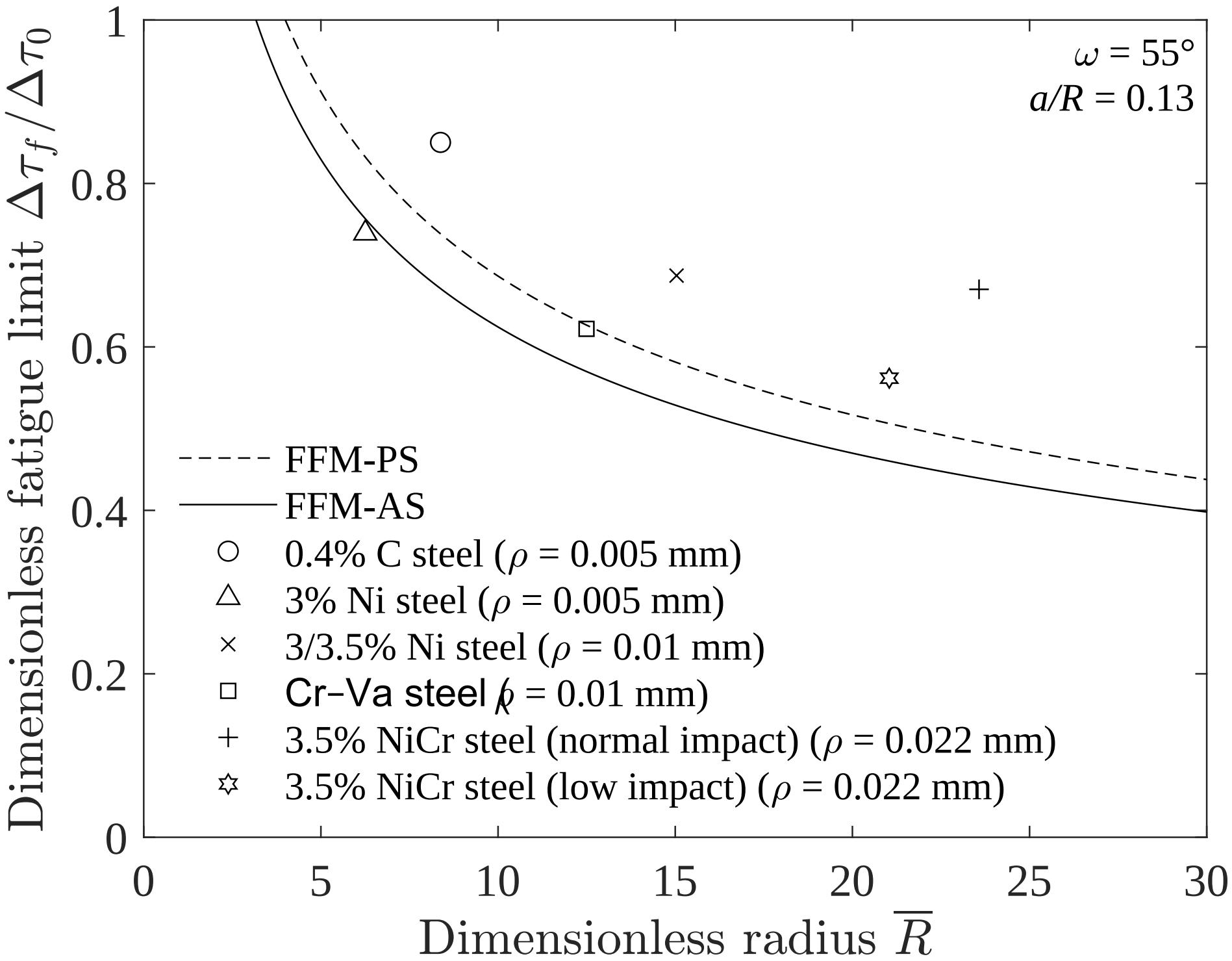

Figure 11

Click here to access/download;Figure;Fig. 11.eps

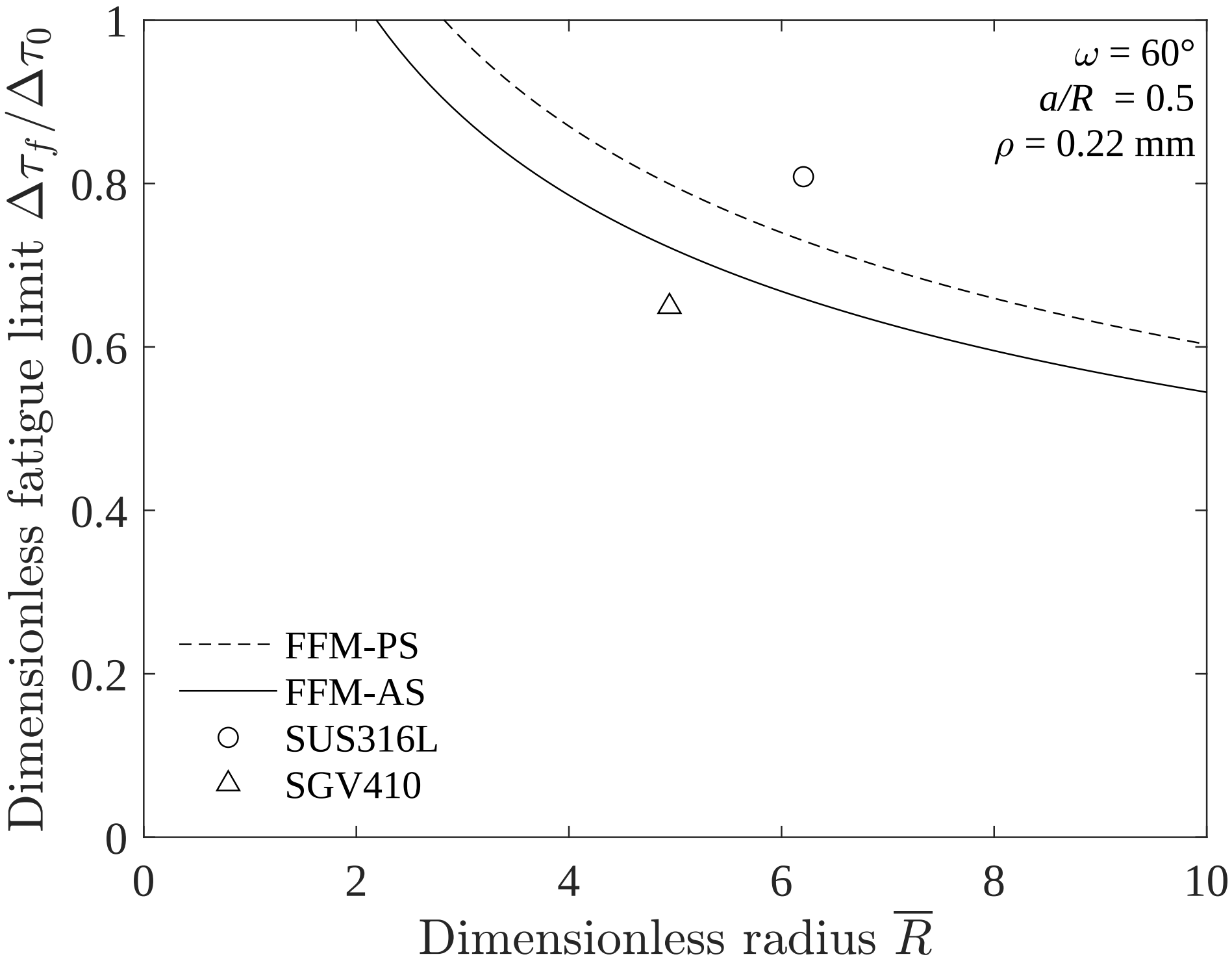

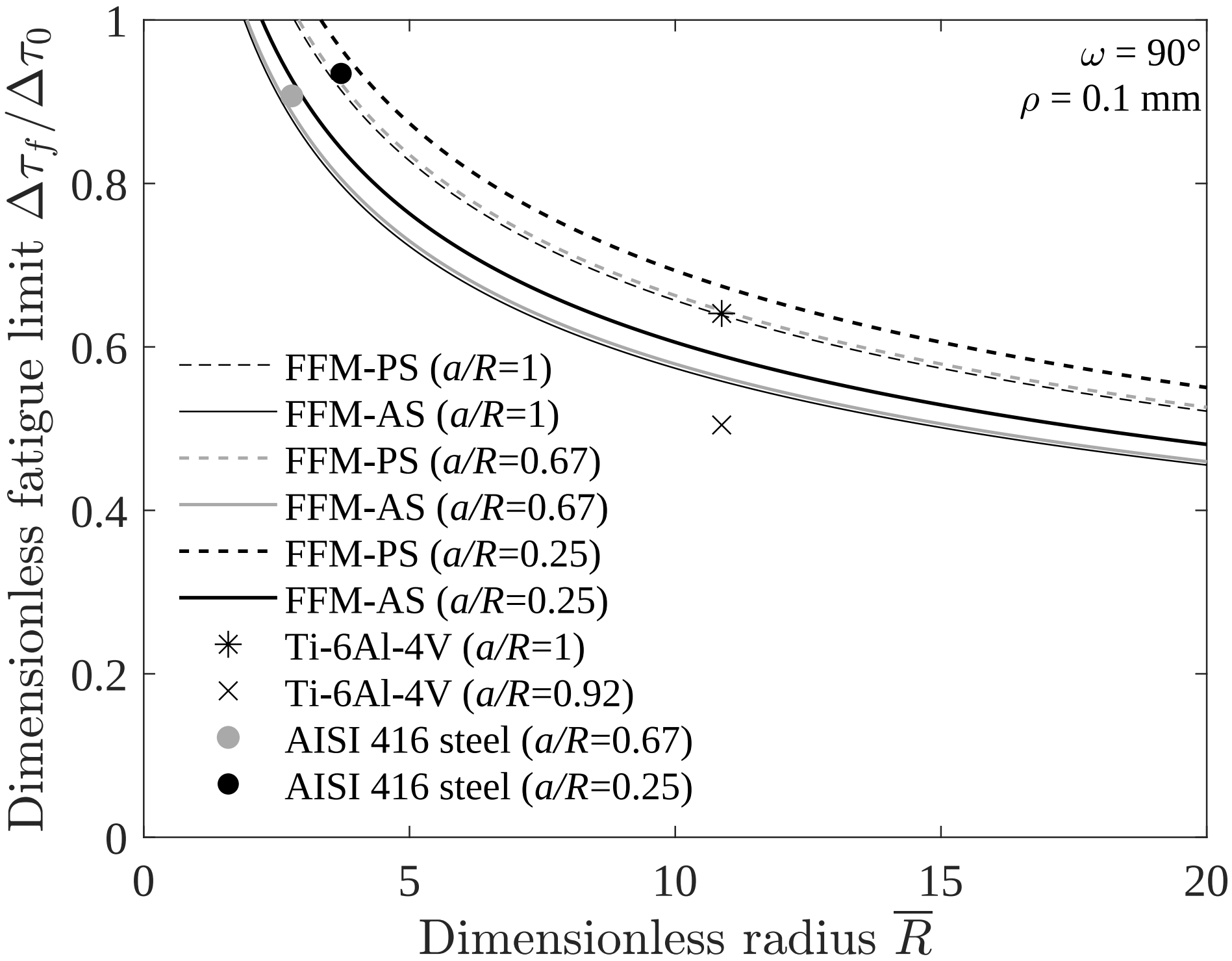

Declaration of interests

☒The authors declare that they have no known competing financial interests or personal relationships that could have appeared to influence the work reported in this paper.

☐The authors declare the following financial interests/personal relationships which may be considered as potential competing interests: